INFORMATION TO USERS

This manuscript has been reproduced from the microfilm master. UMI films the text directly from the original or copy submitted. Thus, some thesis and dissertation copies are in typewriter face, while others may be from any type of computer printer.

The quality of this reproduction is dependent upon the quality of the copy submitted. Broken or indistinct print, colored or poor quality illustrations and photographs, print bleedthrough, substandard margins, and improper alignment can adversely affect reproduction.

In the unlikely event that the author did not send UMI a complete manuscript and there are missing pages, these will be noted. Also, if unauthorized copyright material had to be removed, a note will indicate the deletion.

Oversize materials (e.g., maps, drawings, charts) are reproduced by sectioning the original, beginning at the upper left-hand corner and continuing from left to right in equal sections with small overlaps.

Photographs included in the original manuscript have been reproduced xerographically in this copy. Higher quality 6" x 9" black and white photographic prints are available for any photographs or illustrations appearing in this copy for an additional charge. Contact UMI directly to order.

ProQuest Information and Learning
300 North Zeeb Road, Ann Arbor, MI 48106-1346 USA
800-521-0600

UMI®

ELECTRONIC STRUCTURE AND OPTICAL PROPERTIES OF QUANTUM DOTS

by

THIQUE HUONG NGUYEN

A dissertation submitted to the Graduate Faculty in Physics in partial fulfillment of the requirements for the degree of Doctor of Phylosophy

The City University of New York

2001

This manuscript has been read and accepted for the Graduate faculty in Physics in satisfaction of the dissertation requirement for the degree of Doctor in Philosophy.

8/27/01
Date

Chair of the Examining Committee
Joseph L. Birman
Distinguished Professor of Physics
Department of Physics
The City University of New York

9/04/01
Date

Executive Officer
Louis Celenza

Herman Cummins
Distinguished Professor of Physics
Department of Physics
The City College of The City University of New York

Joel Gersten
Professor of Physics
Department of Physics
The City College of the City University of New York

Melvin Lax
Distinguished Professor of Physics
Department of Physics
The City College of the City University of New York

Fred Pollak
Distinguished Professor of Physics
Department of Physics
Brooklyn College of the City University of New York

David Schmeltzer
Professor of Physics
Department of Physics
The City College of the City University of New York

Supervisory Committee

The City University of New York

Abstract

ELECTRONIC STRUCTURE AND OPTICAL PROPERTIES OF QUANTUM DOTS

by

Thique Huong Nguyen

Adviser: Professor Joseph L. Birman

Because of complete (three dimensional) confinement, quantum dots have a most dramatic quantum size effect. Due to the finite size of the dot, the conduction and valence bands of semiconductor dots are quantized and quantum dot spectra exhibit a series of discret electronic transitions and depend strongly on the size of the nanocrystal.

In this thesis we study the electronic structure and the optical properties of semiconductor quantum dots and semiconductor quantum dot systems. Different properties and different dots and dot systems are described.

The first topic is the electric polarization in a semiconductor dot (II-VI compound). A simple theoretical model for the origin of spontaneous polarization in single nanocrystals is developed, based on the proposal that the origin of the spontaneous polarization is in the strained layer between "cap" and the nanocrystal. The internal electric field in the dot is due to the piezoelectric effect caused by the strain existing in the interface region of material with different lattice constants. Based on spherical rotation symmetry without inversion SO(3), the model employs a distribution of polarization

with symmetry which is a subgroup of SO(3), consistent with the hexagonal structure of wurtzite structure.

The second topic we study is a distribution of many quantum dots, which are arranged together in an array. We present a new model to implement organic exciton-inorganic(semiconductor) exciton hybridization. We consider embedding a quantum dot array into an organic medium. A Wannier-Mott transfer exciton is formed when the exciton in each semiconductor dot interacts via multipole-multipole coupling with other excitons in the different semiconductor dots of the array. A new hybrid exciton appears in the system owing to strong dipole-dipole interaction of the Frenkel exciton of organic molecules with the Wannier Mott transfer exciton of the quantum dot array. This hybrid exciton has both a large oscillator strength (Frenkel-like) and a large exciton Bohr radius (Wannier-like). At resonance between these two types of excitons, the optical non-linearity is very high and can be controlled by changing parameters of the system such as dot radius and dot-dot spacing.

As the third topic, which differs from the pure nanocrystal in the above study, we also present our study on Mn- doped semiconductor nanocrystals such as the ZnS:Mn quantum dot. The effect of an extra electron "injected" into the doped quantum dot with a substitutional Mn^{2+} at the center is considered. The electron confined in the dot will be strongly coupled by exchange interaction with the Mn ion, and will split and mix Mn crystal-field energy levels. As a result, this will strongly break the previous selection

rules. The optical transition of interest is the ${}^4T_1 - {}^6A_1$ transition. Using this model we evaluate the energy structure, wavefunctions, luminescent efficiency and transition life time of a Mn doped quantum dot and compare our results with experimental data.

This work is dedicated to my beloved parents, Nguyen Thanh Long and Le Thi Minh Nguyet, who loved me and had always encouraged me, but could not live until these days.

ACNOWLEDGEMENTS

I am deeply indepted to my thesis advisor, Prof. Joseph L. Birman for his academic guidance, encouragement, advice in my dissertation as well as in many other sides of my graduate student years. I am very grateful to him for his deep knowledge,for his respectation to creativity of his students, for him always being there for us when we need him, for his treating students as if we are in a big family and for a pleasant working environment in our group. With his guidance in these years, I grew up in many aspects and I always feel grateful.

I am grateful to Professors in the Physics Department of City College for their education , advice and discussion, especially Prof. Herman Cummins, Prof. Bunji Sakita, Prof. Melvin Lax, Prof. David Schmeltzer, Prof. V. P. Nair, Prof. Joel Gersten, Prof. Timothy Boyer.

I would like to thank Dr. Al. Efros, Dr. David Norris for their discussion and collaboration, especially Dr. Al. Efros for collaboration in chapter V of this thesis.

I want to thank Prof. Nguyen Ai Viet for his support and encouragement.

Many thanks to visitors of our group: Prof. Anatoly Kuklov, Prof. Shmuel Goshen, Prof Natalya Zymbovskaya for their discussion and encouragement.

I also want to thank my graduate student fellows: Dr. Nina Abrazon, Dr. Meng Lu, Dr. Alexei Bulatov, Dr. Ping Sun, Mr. Len Tevlin for their

friendship, their help and support.

Last, but not least, I would like to give special thanks to my sister Hoa Hong Nguyen and my husband Anh Quoc Nguyen for their love, understanding , patience, encouragement and support in all these years. To me, they are not only my family, but also my best friends and colleagues.

Contents

List of Figures

Chapter 1

INTRODUCTION

Present experiments and theoretical investigations in semiconductor physics appear to be concentrated on the physics of reduced dimensional systems. Over the past several decades, the two-dimensional (quantum wells), one-dimensional (quantum wires) and zero-dimensional (quantum dots) semiconductor systems have been made artificially and studied very intensively. The reduced dimensional semiconductor structures show many new unique properties that are completely different from the bulk semiconductors and have never been observed before. Theoretical and experimental studies show the sensitive dependence of the electronic structures and the optical properties of the semiconductor mesoscopic structures on their size. When the size of these structures are comparable to the electron-hole effective Bohr radius, the quantum wells, quantum wires and quantum dots are called two-dimensional, one-dimensional and zero-dimensional confined systems, respectively. Then the motion of the carriers like electrons and holes is quantized due to the

boundary condition of the material. This quantization gives rise to many interesting phenomena in the confined structures and is called the "quantum size effect".

Being confined in all three dimensions, quantum dots have the biggest quantum size effect and are very attractive objects for for both basic research and application [1-21].

In this thesis, we investigate several optical properties of the quantum dot for different cases: the pure dot, the system of many dots and the dot doped by an impurity.

In chapter 2 we will give some introduction to the theoretical and experimental results on the electronic structure and energy as well as the optical properties of semiconductor quantum dots.

From chapter 3 to chapter 5, some models and theories are presented to explain some experimental results and predict some new results. In chapter 3 our model of the origin of the polarization which is observed in polar nanocrystals is decribed. The theory of piezoelectricity originating in the surface of the nanocrystal is used to explain the existence of the internal electric field inside the quantum dot. A case of particular interest is the dot coated by another semiconductor.

The theory of the hybrid exciton in the quantum dot array is given in chapter 4. In our model, when we place an array of semiconductor quantum dots in an organic host, the transfer Wannier- Mott exciton of the dot array

couples with the Frenkel exciton in the organic medium. This will give rise to the formation of some new kind of exciton, the hybrid, with both large Bohr radius and large oscillator strength. It is shown this leads to an enhanced non-linear optical response.

In chapter 5, we present an entirely new mechanism to control the optical transition by means of doping a quantum dot. We consider the spin-forbidden transition ${}^4T_1 - {}^6A_1$ transition of the Mn^{2+} impurity ion in the doped nanocrystal $ZnS : Mn^{2+}$. We examine the effect that an extra electron inside the quantum dot can produce in changing the transition. Our theory claims that the extra electron in the dot will strongly couple with the d^5 electrons involved in the transition and strongly break the old selection rule: this will transform the forbidden transition into an allowable one. We calculate the energy levels and the new mixed wavefunction of the new states, and then we have the result for the oscillator strength and lifetime to compare with experiment. The calculated lifetime is shortened but not as much as some controversial experiments have claimed.

Chapter 2

EXCITONS IN QUANTUM DOTS

In this chapter we will review some theoretical models as well as some electronic and optical properties of quantum dots as background for our work in chapters 3-5.

2.1 A Spherical Quantum Dot- A Particle-in-a-Sphere Model

The simplest model for a quantum dot is a semiconductor (such as III-V or II-VI, GaAs, ZnS, CdSe...) sphere embedded in glasses or organic material (Fig. 2.1) [1-11]. We will consider the cases where the radius of the quantum dot is larger than the lattice constant of the bulk semiconductor. In a bulk crystal the state of an electron can be obtained by solving the Schrodinger

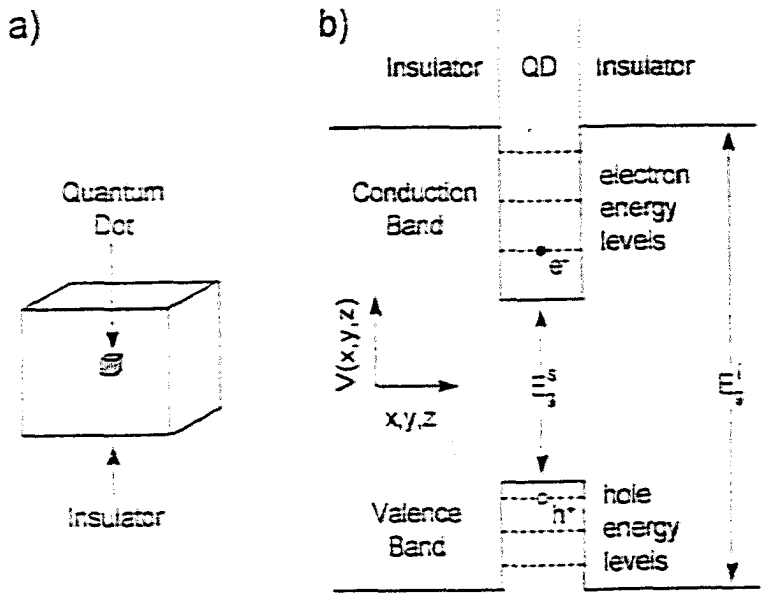

Figure 2.1: *A quantum dot in an insulating material for type I with direct band gap (After D. Norris et al.[19])*

equation with the periodic potential in the Bravais lattice [14]. The electron eigenstate then is written in the Bloch form

$$\psi_{n,k}(r) = e^{ikr} u_{n,k}(r) \tag{2.1}$$

where e^{ikr} is the plane wave and $u_{n,k}(r)$ is periodic with the Bravais lattice vector. The energy eigenvalues of the Schrodinger equation will be $E_n(k)$ where n is the band index, k is the wave vector. With k in the first Brillouin zone near an extremum $E_n(k)$ will be given as:

$$E_n(k) = \frac{\hbar^2 k^2}{2m_{eff}} \tag{2.2}$$

where m_{eff} is the effective mass of the electron or the hole.

For direct gap semiconductors, in the simplest approximation, a nanocrystallite can be considered as a semiconductor sphere of radius R surrounded by an infinitely high potential barrier[6,7] For a particle inside a spherical potential well of radius R_0

$$\begin{aligned} V(r) &= 0 \quad r < R_0 \\ &= \infty \quad r > R_0 \end{aligned} \tag{2.3}$$

In the framework of the envelope function approximation[15] the Schrodinger equation has the solution for a wavefuntion for an electron (or a hole)

$$\Phi_{nlm}(r,\theta,\phi) = Y_{lm}(\theta,\phi)\sqrt{\frac{2}{R_0^3}}\frac{j_l(\chi_{nl}r/R_0)}{j_{l-1}(\chi_{nl})}. \tag{2.4}$$

where $Y_{lm}(\theta,\phi)$ is a spherical harmonic, j_l are the spherical Bessel functions, χ_{nl} are the n-th zero of the spherical Bessel function of the order l.

The requirement (boundary condition) that the wavefunction has to vanish at the sphere surface $r = R_0$ determines the energy eigenvalues of the

particle

$$E_{nl} = \frac{\hbar^2}{2m_{eff}} \frac{\chi_{nl}^2}{R_0^2} \tag{2.5}$$

The first roots of the spherical Bessel function are $\chi_{1S} = \pi$, $\chi_{1p} = 4.493$, $\chi_{1d} = 5.763$...So the lowest energy level of the confined particle is

$$E_{10} = \frac{\hbar^2}{2m_{eff}} \frac{\pi^2}{R_0^2} \tag{2.6}$$

The energy of the confined electron or confined hole in a quantum dot takes discrete values due to the quantization following the spherical boundary condition. It depends on the square of the inverse radius R_0. We also can say that the energy has the same form as the energy (2.2) of the free particle, only here the wave vector is quantized by the spherical boundary conditions.

2.2 Excitons in nanocrystals

We consider a semiconductor where an electron and a hole were created, for example by light, with the electron in the conduction band and the hole

in the valence band. When the electron and the hole approach each other and interact via screened Coulomb attraction, they form a bound state with the energy slightly below the band gap. We understand that the band gap energy is that for which the electron and the hole are separated from each other and no longer experience the Coulomb interaction. This electron-hole bound state is described by the hydrogenic Hamiltonian

$$\hat{H} = -\frac{\hbar^2}{2m^e_{eff}}\nabla_e^2 - \frac{\hbar^2}{2m^h_{eff}}\nabla_h^2 - \frac{e^2}{\epsilon|r_e - r_h|} \tag{2.7}$$

m^e_{eff} and m^h_{eff} are the effective mass of the electron and the hole, respectively, which is small in comparison with the real mass of the electron and the hole. ϵ is the dielectric constant, which is in the range of 5-15 for semiconductors. The small effective masses lead to the large kinetic energy of the electron and the hole, while the large dielectric constant makes the Coulomb interaction between the electron and the hole screened. This makes the exciton have a large separation between the electron and the hole positions, or a large exciton radius.

When the Coulomb interaction between an electron and a hole in the nanocrystal is larger than the size-quantization energies of the electron and the hole, the quantization of the exciton appears[13]. In other words, the exciton is said to be confined in the quantum dot when the size of the dot

approaches the exciton Bohr radius $a_B = \frac{\hbar^2 \epsilon}{\mu_{exc} e^2}$ where μ_{exc} is the electron-hole pair reduced mass. This size is called the molecular limit. Then the electron-hole pair state can be expressed by the wavefunction of the exciton

$$\Psi_{nlm} = \sum_j F_{nlm}(j)\phi(j_r)W_j^c(r_j)\prod_{i\neq j} W_i^v(r_i), \tag{2.8}$$

where W_i^v, W_j^c are Wannier functions of valence band and conduction bands, respectively, and F_{nlm} is the envelope function of the center-of -mass motion, given by

$$F_{nlm}(R,\theta,\varphi) = Y_{lm}(\theta,\varphi)\sqrt{\frac{2}{R^3}}\frac{j_l(\chi_{nl}\frac{r}{R})}{j_{l+1}(\chi_{nl})} \tag{2.9}$$

$\phi_{1s}(r)$ describes the electron-hole relative motion with $j_r = j - j'$.

$$\phi_{1s} = \left(\frac{1}{\pi a_B^3}\right)^{1/2} e^{-r/a_B} \tag{2.10}$$

The site index $j = (j_x, j_y, j_z)$ and $j' = (j'_x, j'_y, j'_z)$ are positive intergers.

Then the energy of the exciton in the quantum sphere is given similarly to Eq. (2.5)

$$E_{nl} = E_g - E^b_{exc} + \frac{\hbar^2}{2M_{exc}} \frac{\chi^2_{nl}}{R_0^2} \tag{2.11}$$

where E_g is the band gap, $E^b_{exc} = \mu_{exc} e^4 / 2\hbar^2 \epsilon^2$ is the exciton binding energy, $\mu_{exc} = m_e m_h / (m_e + m_h)$ is the reduced mass of the electron-hole pair. M_{exc} is the exciton mass, $M_{exc} = m^e_{eff} + m^h_{eff}$.

From (2.11), the energy of the exciton in the sphere takes discrete values and is proportional to the inverse of the square of the sphere radius R_0, and so is strongly dependent on the size of the sphere. Then the energy to separate the electron and the hole (i.e the "effective band gap") will increase in a quantum dot with respect to the bulk semiconductor by the value

$$\Delta E = \frac{\hbar^2}{2\mu_{exc}} \frac{\pi^2}{R_0^2} \tag{2.12}$$

In (2.9) we gave the envelope function [15]. The periodic part of the wavefunction of the electron and the hole have been approximated by using the two-band semiconductor model. For the periodic factors in the total wave function we use the bulk wave functions. In a direct band gap semiconductor like ZnS with parabolic conduction band and warped valence band, with the maximum of the valence band and minimum of the conduction band posi-

tioned at k=0 in k-space, we recall that near the band extrema $k = 0$ we have a parabolic conduction band which is doubly degenerate. The group theory label of the states including spin is Γ_6. The valence bands are four-fold degenerate labelled Γ_8 and the split-off doubly degenerate Γ_7. Because the spin-orbit splitting $\Gamma_8 - \Gamma_7$ is large we neglect the split off band and consider only the exciton states from Γ_6 conduction band and Γ_8 valence band. The angular part of the periodic factors in eqn(2.1) of the four-fold degenerate valence band are given as the following:

$$\begin{aligned} v_{3/2} &= \frac{1}{\sqrt{2}}|(X+iY)\uparrow\rangle, \\ v_{-3/2} &= \frac{i}{\sqrt{2}}|(X-iY)\downarrow\rangle, \\ v_{1/2} &= \frac{1}{\sqrt{6}}|(X+iY)\downarrow -2Z\uparrow\rangle, \\ v_{-1/2} &= \frac{i}{\sqrt{6}}|-(X-iY)\uparrow +2Z\downarrow\rangle. \end{aligned} \tag{2.13}$$

while the functions of the conduction band are

$$\begin{aligned} u_{1/2} &= \frac{1}{\sqrt{2}}|S\uparrow\rangle, \\ u_{-1/2} &= \frac{1}{\sqrt{2}}|S\downarrow\rangle, \end{aligned} \tag{2.14}$$

where the indices $\alpha = 1/2, -1/2, 3/2, -3/2$ in (1.13), (1.14) are the component of the total momentum (spin and orbital) of the electron or holes, quantized on the "z" axis. The expressions (2.13), (2.14) take account of spin by writing the wavefunction as a sum of products of orbital and spin functions, consistent with the double group.

2.3 Oscillator Strength in Quantum Dots

The size quantization effect of the absorption spectrum was studied theoretically and experimentally. In the exciton picture for calculating the absorption coefficient one needs to compute the transition dipole moment from the ground state $\Psi_g$to an excited state Ψ_n [13]

$$\alpha(w) \sim |\langle \Psi_n | P | \Psi_g \rangle|^2 \tag{2.15}$$

where P is a component of the dipole moment operator $\vec{P}$

$$\vec{P} = \sum_i p_i = \sum_i e\vec{r_i} \tag{2.16}$$

with

$$\langle W_{j'}^{c}(r_j)|p_j|W_j^{v}(r_j)\rangle = p_{cv}\delta_{jj'} \tag{2.17}$$

Then the exciton transition dipole moment will have the form

$$\langle \Psi_n|P|\Psi_g\rangle = \sum_j F_n(j)\langle W_j^{c}(r_j)|p_j|W_j^{v}(r_j)\rangle \tag{2.18}$$

The transition dipole moment to the excited state with $n, l = 0, m = 0$ for an exciton in a quantum sphere is

$$\begin{aligned}\langle \Psi_n|P|\Psi_g\rangle &= \int d\vec{R}\Psi_{n00}(\vec{R})\phi_{1S}(0)p_{cv} \\ &= p_{cv}\phi_{1s}(0)2\sqrt{2/\pi}\frac{1}{n}R_0^3\end{aligned} \tag{2.19}$$

We note from here that the oscillator strengths of excitons in a quantum dot are concentrated on the low excited states, when n is small. The oscillator strength is largest for the lowest excited state, eg. for $n = 1$.

2.4 Exciton Fine Structure

The spherical theory [1,2,3] predicted that in ZnS for example the lowest energy electron- hole pair state $1S_{3/2}1S_e$, or the band-edge exciton, is 8- fold degenerate. We recall the doubly degenerate Γ_6 conduction band and the Γ_8 four-fold degenerate valence band will give 8 exciton states. However,the deviation from the spherical model such as the effect of the "nonspherical" shape[9-10] and internal structure of the crystal dot, as well as the electron-hole exchange interaction [16] was also predicted by the theory. These effects will split the band-edge exciton into sublevels [18-22]. The structure was also observed within the first absorption feature in [17] and implied the existence of the structure of the band-edge exciton [17,18].

These effects split the energy levels of the band-edge exciton into sub-levels. Theoretically, these effects are counted as small perturbations to the spherical model. In the larger dot, where the nonspherical shape of the nanocrystal and the anisotropy of the crystal are more important, the exchange interaction between the electron and the hole is considered to be small. Then, the band-edge exciton splits into two 4-fold degenerate states [9] due to the reduction from spherical to uniaxial symmetry. When the quantum dot is smaller, due to confinement of the electron and the hole, the overlap between the wavefunction of the electron and the hole increases and the electron - hole exchange effect becomes more important and the effect

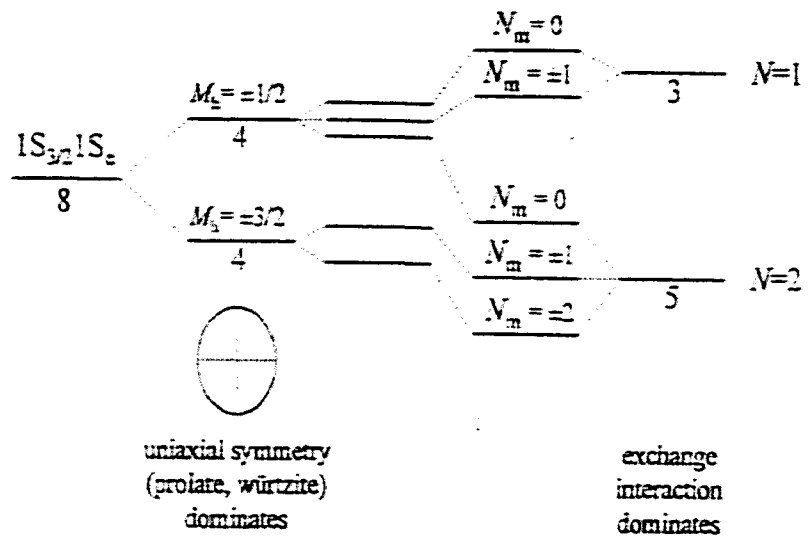

Figure 2.2: *Energy level diagram of the exciton fine structure (after Norris et al, [21])*

of the nanocrystal shape is less. In this case the total angular momentum is the principal quantum number, and the band exciton splits into two states: a 5-fold degenerate N=2 state, and 3- fold degenerate N=1 state. In the intermediate size of the quantum dot, when both effects are included, the band-edge exciton splits into five states. The good quantum number in this case is the projection of the total angular momentum along the z-axis N_m. The five states are:one two-fold sublevel with $N_m = \pm 2$, two two-fold sublevel with $N_m = \pm 1$, and two single states with $N_m = 0$.

In Fig.2.2 is the diagram for this splitting, depending on the size of the nanocrystal, is shown [21].

In the electric dipole approximation the emission from the lowest band-edge exciton state $N_m = 2$ is optically forbidden. Because of this, the state is called the "dark exciton". Relaxation of the electron-hole pair into this intrinsic, band-edge state, where the electron-hole pair can stay for a long time, can explain the long radiative lifetime observed in CdSe quantum dots. The transition from this state $N_m = 2$ to the ground state is one-photon forbidden, but a phonon-assisted transition can occur, explaining the stronger LO- phonon coupling of the emitting state and resulting the long radiative lifetime [21].

2.5 Doping nanocrystals

In bulk II-VI compounds, doping is used to obtain efficient luminescent materials for many applications. To further exploit the advantage of the quantum nanocrystal, efforts have been made to study the properties of certain impurity ions in the nanocrystal. An impurity in the quantum dot was introduced by several groups [61, 67, 68, 69, 70, 71] with many interesting properties. Because of the confinement, the structure of the impurity level, and also the interaction of the impurity with the host all will change, and so the optical properties such as the probability of the optical impurity transitions, and the transition efficiency are expected to have big changes. Nanocrystals doped with transition metal or rare-earth elements have decreased concentration

quenching effect since the resonant energy transfer among the luminescent centers is controled by the boundary of the nanocrystal.

Nanocrystals of ZnS doped with Mn have been claimed [61, 62] to have very strange properties. The doped nanocrystals were prepared by precipitation after reaction in toluene. Since nanocrystals sinter at extremly low temperature, the authors [61] doped the nanocrystal during precipitation. To dope the ZnS, manganese chloride is reacted with ethylmagnesium chloride to form diethylmanganese in a solvent, and then added to the reaction. The separation of the particles is maintained by coating with the surfactant metallic acid. The optical properties of these doped nanocrystals are then studied at room temperature with the band to band excitation to excite the Mn^{2+} emission. This particular system is claimed to exibit remarkable optical properties. Photoexcitation occurs via the s-p states of the nanocrystal, the excitation is transferred to the d states of the Mn ion, and then the emission can take place by transition between the d levels. But this optical process has high efficiency and a luminescence lifetime several orders of magnitude faster than in bulk ZnS:Mn.

The spin-forbidden ${}^4T_1 - {}^6A_1$ was particularly studied and a shortening of the luminescent lifetime from 1.8 ms to 3.7 ns was reported when the system changes from ZnS:Mn in bulk to ZnS:Mn in a doped nanocrystal. Also, the enhancement of the radiative efficiency is observed to increase and to depend strongly on the size of the nanocrystals.

Many explanations have been proposed for this strange effect[66, 71, 73]. Among them is the enhanced hybridization of the s-p state of the host and the d-state of the Mn ion[66]. It would enhance the transfer of the excitation. Another possibility is some surface effect on the Mn ion. But up to the present, there is no accepted mechanism for this effect. Actually, the problem now has produced a controversy as other experimental groups claimed they have not observed the same shortening of the lifetime for this transition. This will be studied in chapter 5. [74].

Chapter 3

POLARIZATION IN POLAR NANOCRYSTALS

In this chapter we propose the piezoelectric effect due to mismatch of lattice constants in the surface of the nanocrystal as the origin of the permanent polarization and the internal electric field, which are observed for the nanocrystals[25].It gives good agreement with experiment.Other explanations were also proposed.

3.1 Introduction

As described above, the spherical quantum confinement model with the effective mass approximation and an approximate treatment of the Coulomb interaction[1,2] is presently accepted as the best model to describe the quantum dot and the size-dependence of the optical properties of the quantum

dot. The absorption features and their size dependence are well described by this model [5,12,17]. Also, the observable fine structure of the band-edge exciton was predicted to result from the additional effects such as the non-spherical shape of the dot and the exchange interaction between the electron and the hole [18,19].

However, some observations give results indicating that there should be additional modification of the spherical model of nanocrystals [19, 22]. The Stark measurement [23] suggested the presence of a large change in the dipole moment during optical excitation. The detailed comparison [26] of one- photon and two-photon band edge spectra of CdSe nanocrystals suggests the presence of the internal electrical polarization[28-31] which lifted the inversion symmetry. Some studies of colloidal CdSe nanocrystals by coating a CdSe surface with a layer of ZnS before capping with an organic base show a significant increase of photoluminescence quantum efficiency. The increase of photoluminescence partly can be explained by the difference of the band gaps (ZnS has a higher band gap than CdSe), but may also imply the existence of some "internal electric field", which mixes the optical energy levels.

3.2 Existence of a Permanent Dipole Moment in a CdSe Quantum Dot

Recently, P. Guyot-Sionnest and coworkers [30] researched the one-photon and two-photon excitation transitions, and observed the similarity of one-photon and two-photon spectra in CdSe nanocrystallites. But in the two-photon spectrum, the transition $1S_{3/2} - 1S_e$, which is parity-forbidden, has been found. Observation of the parity-forbidden transition strongly indicates that a spontaneous polarization exists in the CdSe nanocrystal, that is, some internal electric field exists that mixes the odd and even band-edge hole states, as the authors of[30] proposed. It also implies the lack of inversion symmetry of these nanocrystals.

In their later papers [33], these authors have measured the magnitude of this dipole moment by the method of dielectric constants. In their experiment, the CdSe nanocrystals were synthesied by injection of dimethyl cadmium and trioctylphosphine selenide in a hot bath of trioctylphosphine and trioctylphosphine oxide. The size dispersion is further reduced by fractional precipitation to the size dispersion between $5\% - 10\%$. The authors get the diameters of 34Å and 46Å for two different kinds of nanocrystals.

The complex dielectric coefficient

$$\epsilon = \epsilon' - i\epsilon'' \tag{3.1}$$

has the real and the imaginary parts relating to the dipole dielectric contri-

bution following Debye's formula [33] as:

$$\epsilon' = \epsilon'_e + \frac{\epsilon_d}{1+(w\tau)^2}$$
$$\epsilon'' = \frac{\epsilon_d}{1+(w\tau)^2} w\tau \qquad (3.2)$$

where $\tau = 4\pi\eta r_H^3/kT$ is the relaxation time and $\epsilon_d = 4\pi n\mu^2/3kT$ is the dipole dielectric contribution. μ is the screened dipole moment, r_H is the hydrodynamic radius, which is close to the radius of the semiconductor semiconductor plus its capping layer. ϵ'_e is a constant and η is the viscosity of the solvent.

Table I give results of their measurement. In [33] the authors obtained the dipole moments of 25 debye for the 17 Åradius nanocrystal and 47 debye for 23 Åradius nanocrystal. In the later paper [35], they report even larger values of the dipole moments: 66 debye for the 34 Åradius dot and the dipole moment varies between 41-98 debye for the quantum dot sizes they studied.

TABLE I. Results.

Semiconductor radius a	17 Å	23 Å
Screened dipole moment μ	25 ± 2 D	47 ± 5 D
Relaxation time τ_{exp}	$0.27 \pm .03$ μs	0.7 ± 0.2 μs
Hydrodynamic radius r_H	29 ± 1 Å	39 ± 3 Å
τ_{exp}/τ_{theory}	0.9 ± 0.1	1.4 ± 0.4

The measurements of the conductivity showed that this dipole moment cannot be accounted for by the nanocrystal charge and indicated that the measured dipole is an intrinsic property of an uncharged nanocrystal and exists permanently by itself in the nanocrystal. Also, the measurement of the dipole moment at different temperature shows that there is no thermal effect on the dipole moment.

We use the formula for the internal polarization[37]

$$P_0 = \mu(2\epsilon_1 + \epsilon_2)/4\pi R_0^3\epsilon_1 \tag{3.3}$$

where ϵ_1 and ϵ_2 are the static dielectric constant of the surrounding matrix and nanocrystal, respectively, then the value of the internal polarization of 0.7 and 0.9 $\mu C/cm^2$ is obtained for the 23 Åand 17 Å- radius nanocrystals, respectively. This result also implies the strong size dependence of the internal polarization.

In Fig.3.1 the size dependence of the dipole moment reported by [35] is shown. We see that the dipole moment is increasing linearly with the dot radius.

Until now there is still no definite answer for the origin of the permanent dipole moment in the nanocrystal. Brus and coworkers [27] show that the dipole moment is extremly sensitive to the detailed atomic structure and suggest that the origin of the dipole moment may be the lifting of the inversion symmetry in the hexagonal lattice. Also recently, Brus and coworkers

6962 J. Chem. Phys., Vol. 111, No. 15, 15 October 1999

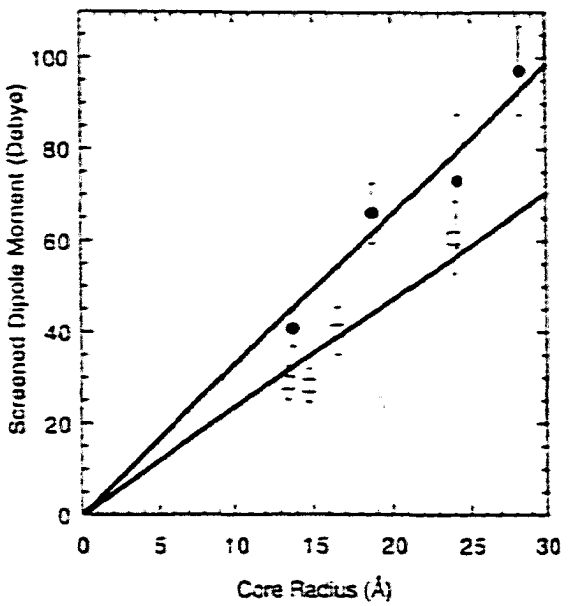

Figure 3.1: *Size dependence of the dipole moment for CdSe*

[27] measured the electrostatic charge and photoionization characteristics of a single CdSe nanocrystal and came to the conclusion that the nanocrystal is initially charged neutral as prepared, but upon photo excitation, it develops a positive charge, and the ionization rate depends linearly on the laser density producing the photoexcitation. They propose the ionization as a model for origin for the permanent dipole of the dot, but since the lifetime of the positive charge due to laser photoionization is different from the "infinite lifetime" of the permanent dipole, they suggested that two kinds of charged states can exist.

Guyot-Sionnest and coworkers [35] also suggest that the thermal induced charging may be one origin of the dipole moment.

In this chapter we want to examine another model, namely the model of the piezoelectric effect originating on the surface of the nanocrystal as the origin of the permanent electric polarization and electric internal field inside the nanocrystal.

3.3 Structure of CdSe Nanocrystals

The electronic structure and optical properties of nanocrystals have been described by by the spherical confinement approximation. So, the question about the real structure and symmetry of the nanocrystal is important to be considered. The deviation from spherical symmetry due to crystal structure (intrinsic hexagonal) would be some small perturbation to the model, and may lead to some changes in energy spectra or the selection rules of optical transitions.

The authors of [28] showed a micrograph of CdSe nanocrystal from high-resolution electron microscopy (HREM) and resonance spectroscopy. Their HREM data were collected on a sample of average diameter 65A. They were able to view nanoocrystals from different directions(Fig.3.2).

As the result of this work, the hexagonal shape of the nanocrystal was reported. The top and bottom sufaces terminate in polar (001) and $(00\bar{1})$. The (001) surface is purely cadmium terminated whereas the $(00\bar{1})$ is purely selenium. The resonant Raman depolarization data showed that the point

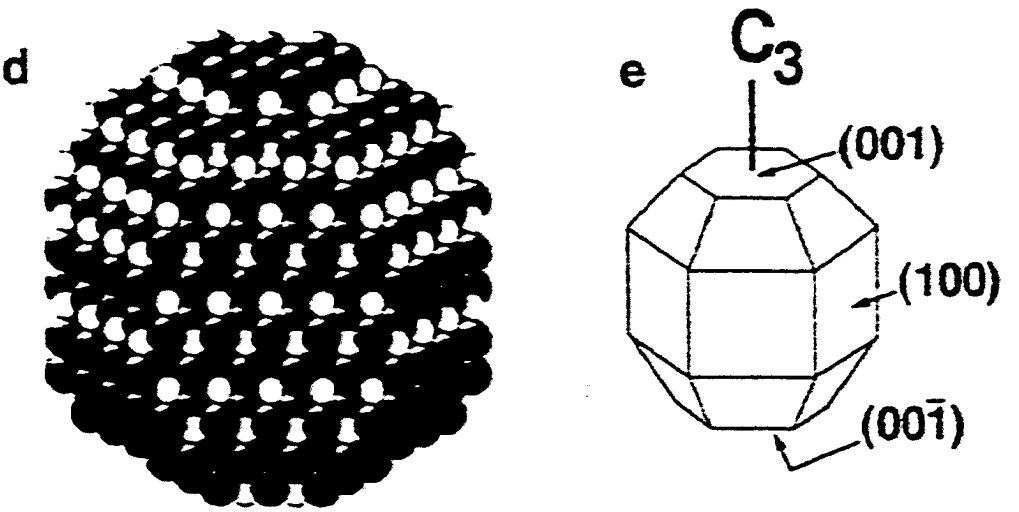

Figure 3.2: *a)HREM micrograph of CdSe nanocrystal viewed along [001] zone axis (c-axis) of the wurtzite lattice. b)A nanocrystal viewed along the [010] zone axis (perpendicular to the c-axis)*

group symmetry of electronic states of CdSe nanocrystal is not T, but rather are A and E. The fact that the triply degenerate T state splits into A and E states supports the point group assignement of C_{3v} for wurtzite CdSe nanocrystal

So, a CdSe nanocrystal has an hexagonal structure with a top purely cadmium terminated surface and a bottom purely selenium surface. It means that the CdSe nanocrystallite itself has no inversion symmetry. And of course, the coated CdSe nanocrystallite has no inversion symmetry either.

3.4 Model for the Polarization- The Piezoelectric Effect

The fact that the CdSe nanocrystal has the top surface purely Cd while the bottom surface is purely Se is very important. Namely, when the CdSe nanocrystal is capped by another semiconductor shell, the Cd and Se in the top and bottom surface of the nanocrystal will couple with the ions of the shell to form thin layers of different materials in the top and bottom surface of the nanocrystal.

For a clear picture, we consider a CdSe nanocrystal capped by a ZnS shell and model the absence of inversion symmetry by the layer model in Fig.3.3. The ZnS semiconductor also can be described by the layer structure: a layer of Zn is continued by a layer of S, and again Zn, and so on. For CdSe coated by ZnS (Fig. 3.3a) we draw the layers of Cd, Se, Zn, S in detail. In the top and bottom surfaces of CdSe nanocrystal, the layers of the elements are in inverse order (Fig. 3.3b). The Cd layer (top layer of the nanocrystal surface) and S layer (the bottom layer of the ZnS shell) in the interface of CdSe and ZnS at the top surface are placed next to each another and can be considered as being coupled together, and so we have a thin layer of CdS in the top surface of the dot. With the same assumption, the Se layer (bottom layer of the nanocrystal surface) and the Zn layer (the top layer of the shell) in the CdSe-ZnS interface at the bottom surface are placed next to each

another and can be considered as coupling together to form a thin layer of ZnSe in the bottom surface of the nanocrystal (Fig.3.3c). The materials of those thin layers are different from each another as an additional indication for the absence of the inversion symmetry. Also, the materials of those thin layers are different from the material of the semiconductor shell, and the difference between the lattice constants of neighbor materials can lead to some strain existing on the surface of the nanocrystal [41].

Based on this model we propose here a simple theory to explain the existence of the spontaneous polarization in the interface surface of CdSe and ZnS. In the interlayer bounding surface of a nanocrystallite, where different materials interface, there should be a strain caused by the difference between lattice constants of different materials. Because of this strain, the piezo electric effect will produce an electric polarization in the surface layer of the crystallite, which is proportional to the difference of the lattice constants. The lack of inversion symmetry is a condition for the existence of the piezoelectric effect, and all these wurtzite structure materials are piezoelectric. So, originating from the piezoelectric effect, the spontaneous polarization in the surface layer has the form:

$$\mathbf{P} \sim e_{14}\frac{\Delta u}{u}, \tag{3.4}$$

where e_{14} is the piezoelectric constant, u is some lattice constant, Δu - the difference of the lattice constants of materials in surface layers. For simplicity, we take Δu constant; in reality the strain will be distributed, i.e. Δu will be a funtion of z. For CdSe coated by ZnS, the value $\frac{\Delta u}{u}$ is about 10% [39], and the polarization is rather large. We will assume elastic modulus C_{14} has its bulk value in CdSe. Note that we are assuming no free charge in the dot and only the lattice effect is considered.

3.5 Calculation of the Internal Electric Field

To demonstrate how this surface polarization can cause the internal electric field inside the coated dots, we use a simple geometric model, which is very close to the hexagonal structure of CdSe dots, but with higher symmetry (Fig.3.4).

Let us imagine that we have a spherical dot of CdSe, coated by ZnS. At the surface of this dot, where CdSe and ZnS interface, there exists a thin layer, composed of CdS in the upper half of the spherical surface, and ZnSe in the lower half. To be similar to the hexagonal structure of the crystallite, where the polarization due to the piezoelectric effect is nonzero only in the top and bottom horizontal planes (Fig.3.4a), in our spherical model we assume that the piezoelectricity causes a nonzero P_1 only in the part of CdS surface (top) layer with angle θ satisfying $\pi/3 < \theta < 2\pi/3$, and a nonzero P_2 only in the part of ZnSe surface (bottom) where $-2\pi/3 < \theta < -\pi/3$ (Fig.3.4b).

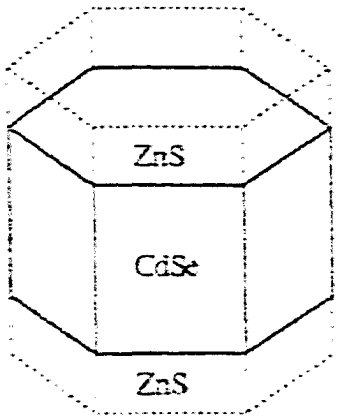

a)

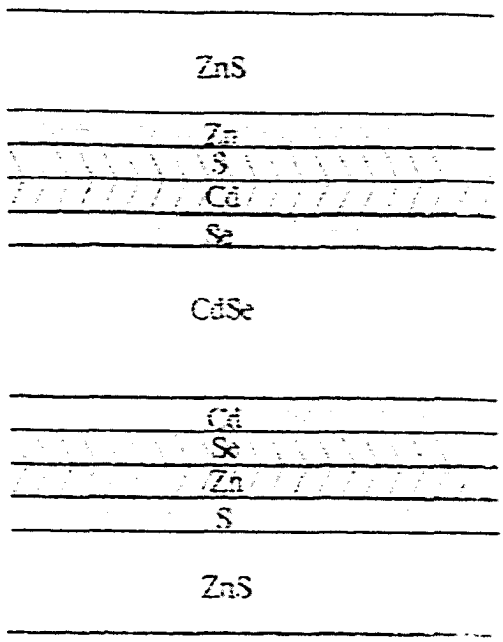

b)

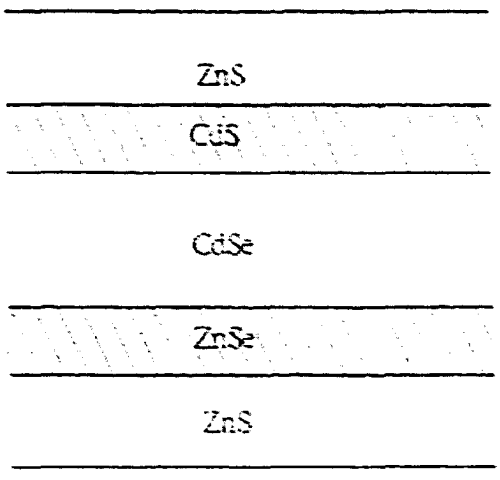

c)

Figure 3.3: *The layer model of the coated crystal showing the position of layers in detail. a) The CdSe dot coated ZnS. b). The layers of elements Cd, Se, Zn, Sn upper and lower surfaces are inverse. c) The element layers in the interfaces couple and make up the thin layers of CdS (top) and ZnSe (bottom) in the interface CdSe-ZnS surfaces*

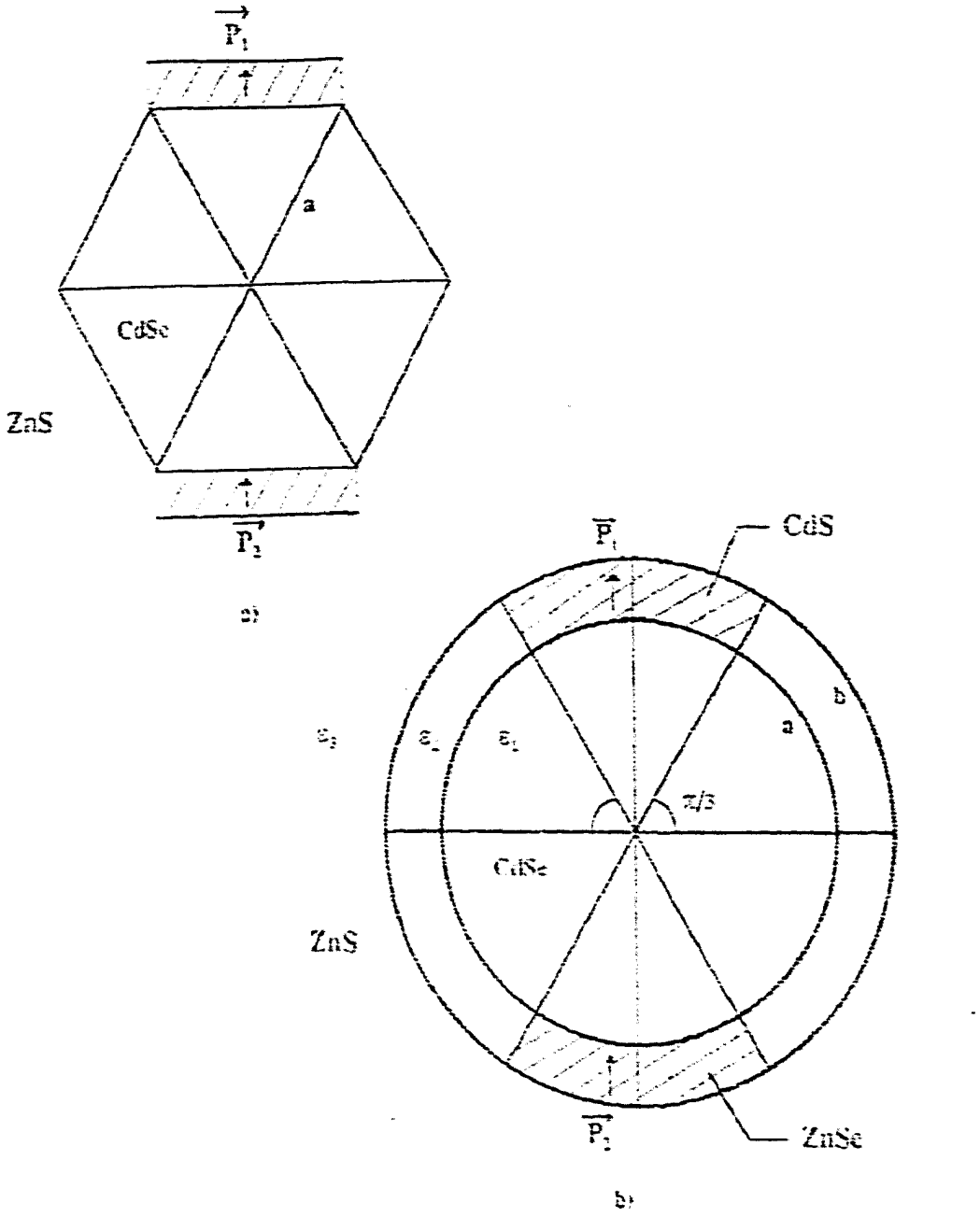

Figure 3.4: *The spherical model illustrating the hexagonal structure of nanocrystal. a) Hexagonal structure of a CdSe quantum dot capped by a ZnS coat. The polarization is different from zero only for the very top and very bottom surface. b) Spherical model. Surface polarization is different from zero only where it exists in the hexagonal structure. CdSe is inside, outside is ZnS, the upper surface layer is CdS and the lower surface layer is ZnSe.*

In all other parts of the surface, the polarization equals zero.

In other word, we write the expression for the polarization in the dot surface:

$$\begin{aligned} \mathbf{P} &= \mathbf{P}_1\Theta(\theta - \pi/3)\Theta(2\pi/3 - \theta), \\ \mathbf{P} &= \mathbf{P}_2\Theta(\theta - 4\pi/3)\Theta(5\pi/3 - \theta), \end{aligned} \tag{3.5}$$

The dielectric constants of the dot, the thin layer and the coat are ϵ_1, ϵ_2, ϵ_3, respectively.

Because of the lack of inversion symmetry, $\mathbf{P}_1$, $\mathbf{P}_2$ will have the same direction.

Now we use the usual electrostatic method to find the internal electric field inside the dot due to the surface spontaneous polarization.

The surface charges due to the polarization in the inside (σ_a) and outside (σ_b) surfaces of the thin layer obey :

$$\begin{aligned} \sigma_a &= \mathbf{P} \cdot \mathbf{n} = P\cos\theta, \\ \sigma_b &= \mathbf{P} \cdot \mathbf{n}' = -P\cos\vartheta, \end{aligned} \tag{3.6}$$

with P given in (3.5).

Due to the symmetry of our model, it is easy to choose the electrostatic potentials and the boundary conditions for this coated dot system. The electrostatic potential for regions inside the dot, in the thin surface layer and in the coat are Φ_1, Φ_2, Φ_3, respectively, which can be expanded in spherical Legendre polynomials:

$$\begin{aligned}
\Phi_1 &= \sum_l \alpha_l r^l P_l(\cos\theta), \\
\Phi_2 &= \sum_l \left(\beta_l r^l + \frac{\gamma_l}{r^{l+1}}\right) P_l(\cos\theta), \\
\Phi_3 &= \sum_l \frac{\delta_l}{r^{l+1}} P_l(\cos\theta).
\end{aligned} \tag{3.7}$$

where r is the distance to the centre of the dot, P_l is a Legendre Polynomial, α_l, β_l, γ_l, δ_l are coefficients, l are non-negative integers. The boundary conditions at the surface a and b of the coated dot require the continuity of tangential components of electric field

$$\begin{aligned}
-\frac{1}{b}\partial\Phi_3/\partial\theta|_{r=b} &= -\frac{1}{b}\partial\Phi_2/\partial\theta|_{r=b}, \\
-\frac{1}{a}\partial\Phi_2/\partial\theta|_{r=a} &= -\frac{1}{a}\partial\Phi_1/\partial\theta|_{r=a},
\end{aligned} \tag{3.8}$$

and the discontinuity of normal components of the displacement

$$\begin{aligned} \epsilon_2 \partial\Phi_2/\partial\theta|_{r=a} - \epsilon_1 \partial\Phi_1/\partial\theta|_{r=a} &= -P\cos\theta, \\ \epsilon_3 \partial\Phi_3/\partial\theta|_{r=b} - \epsilon_2 \partial\Phi_2/\partial\theta|_{r=b} &= P\cos\theta. \end{aligned} \tag{3.9}$$

(3.8) and (3.9) give the system of equations for the coefficients α_l, β_l, γ_l, δ_l of the expressions(3.7). Replacing (3.7) into (3.8) and (3.9) we have the system of equations:

$$\alpha_l b^l = \beta_l b^l + \frac{\gamma_l}{b^{l-1}}$$

$$\frac{\delta_l}{a^{l-1}} = \beta_l a^l + \frac{\gamma_l}{a^{l-1}}$$

$$\left[\epsilon_2 l a^{l-1}\beta_l - \epsilon_2 \frac{(l+1)\gamma_l}{a^{l-2}} - \epsilon_1 \alpha_l a^{l-1}\right] P_l(cos\theta) = -Pcos\theta$$

$$\left[-\epsilon_3 \frac{(l+1)\delta_l}{b^{l-2}} - \epsilon_2 l\beta_l b^{l-1} + \frac{\epsilon_2(l+1)\gamma_l}{b^{l-2}}\right] P_l(cos\theta) = Pcos\theta \tag{3.10}$$

To satisfy all equations in (3.10) simultaneously, all α_l, β_l, γ_l, δ_l with $l \neq 1$ must be zero. Then the electrostatic potential inside and outside the quantum dot will be described by these coefficients follows:

$$\begin{aligned} V_{in}(r) &= \alpha_1 r cos\theta \\ V_{out}(r) &= \frac{\delta_1}{r^2} cos\theta \end{aligned} \tag{3.11}$$

where $V_{in}(r)$ is the electrostatic potential at point r inside the quantum dot, and V_{out} is the electrostatic potential outside the dot. From (3.10) we have a system of equations for $\alpha_1, \beta_1, \gamma_1$ and δ_1

$$\alpha_1 b = \beta_1 b + \frac{\gamma_1}{b^2}$$

$$\frac{\delta_1}{a^2} = \beta_1 a - \frac{\gamma_1}{a^2}$$

$$\frac{2}{3}(\epsilon_2\beta_1 - \epsilon_2\frac{2\gamma_1}{a^3} - \epsilon_1\gamma_1) = (P_1 + P_2)\left(\frac{3\sqrt{3}}{8} - 1\right)$$

$$-\epsilon_3\frac{2\delta_1}{b^3} - \epsilon_2\beta_1 + \frac{2\epsilon_2\gamma_1}{b^3} = (P_1 + P_2)\left(1 - \frac{3\sqrt{3}}{8}\right) \tag{3.12}$$

we have a solution for α_1, the expansion coefficient of the potential inside the nanocrystallite as the following

$$\alpha_1 = -\alpha(P_1 + P_2) \tag{3.13}$$

where

$$\alpha = \left(1 - \frac{3\sqrt{3}}{8}\right) \frac{2(\epsilon_2 - \epsilon_3)a^3b^3 - \epsilon_2 b^6 - 2\epsilon_3 a^6}{2(\epsilon_2 - \epsilon_1)(\epsilon_2 - \epsilon_3)a^3b^3 - (\epsilon_2 b^3 + 2\epsilon_3 a^3)(\epsilon_1 A^3 + \epsilon_2 b^3)}. \tag{3.14}$$

Then the electrostatic potential inside the nanocrystal will be equal to:

$$V = -\alpha(P_1 + P_2)\cos\theta \tag{3.15}$$

It means that the internal electric field caused by the spontaneous polarization in the nanocrystallite dot will be linearly proportional to the sum of $\mathbf{P}_1$ and $\mathbf{P}_2$:

$$\mathbf{E} = \alpha(\mathbf{P}_1 + \mathbf{P}_2) \tag{3.16}$$

So, from (3.4) and (3.16), we have the polarization in the surface and the electric field inside the nanocrystal due to the piezoelectric effect caused by the difference of the lattice constant of the material layers in the dot surface. We will estimate the polarization and the electric field numerically to compare with the experimental results [33]

3.6 Numerical Estimation and Comparison with the Experiments

In order to examine the amplitude of the polarization and the internal electric field, we can evaluate **P** and **E** using standard parameters of CdSe and ZnS [38]. The piezoelectric constant $e_{14} = 4.2 \cdot 10^4 (esu)$ [37],[40]. For the lattice constants of CdSe, CdS, ZnS, ZnSe we take :

$$u(CdSe) = 6.05\mathring{A}, u(CdS) = 5.83\mathring{A}, u(ZnS) = 5.40\mathring{A}, u(ZnSe) = 5.66\mathring{A}$$

so that in the upper surface(interface of CdS-ZnS) $\frac{\Delta u_1}{u_1} = 0.08$, and in the lower surface (interface of ZnSe-ZnS) $\frac{\Delta u_2}{u_2} = 0.05$. Hence, respectively, the polarization in the upper and lower surfaces equal $P_1 = 3.3 \cdot 10^3 (esu)$ and $P_2 = 2.1 \cdot 10^3 (esu)$ (or $P_1 = 1.1 \mu C/cm^2$ and $P_2 = 0.7 \mu C/cm^2$).

Taking dielectric constants $\epsilon_1 = 6.1$, $\epsilon_2 = 5.3$, $\epsilon_3 = 5.2$, for a CdSe nanocrystal of radius $a = 20\mathring{A}$ and the surface thin layer $b - a = 5\mathring{A}$, the

coefficient $\alpha = 0.06$ and the magnitude of internal electric field is about $3.3 \cdot 10^2(esu)$ (or $4.8 \cdot 10^4 V/cm$).The field is rather large, and the effect can be considered important.

At presence there is still no experimental data for the magnitude of electric field of coated dot. But the data of bare CdSe dot can give us some idea. The predicted polarization and electric field are almost of the same magnitude of the data observed in [33,35], with some small difference. The reason maybe lies in the difference between the strain effects of the coated dot and bare dot in organic host. Another possibility, as some authors suggested, is due to the existence of the space charges distributed around the nanocrystal.

3.7 Summary

In summary, we have proposed the piezoelectric effect as the origin of the spontaneous polarization and the large dipole moment in nanocrystallites. We presented a simple model in which we used the absence of inversion symmetry in the structure of a wurtzite nanocrystal in order to evaluate the magnitude of the dipole moment. We obtain a rather large internal electric field existing inside the nanocrystallite. This electric field exists not only in the coated dots, but in all nanocrystallites, which are put into other materials, because of the strain in their surfaces. The existence of the internal electric

field and the absence of inversion will change the electronic structure, mix the optical levels and give new results in one- and two-photon transitions, in the Stark effect of excitons and other optical effects.

The calculation was made for the coated dot. We expect that for the pure semiconductor dot there should exist the strain on the dot surface also due to the mismatch of the lattice distances between the dot's material and the organic coat, but this requires further research.

Just after finishing the work, we received the experimental data [41] confirming the presence of the strain in the core/shell surface. Working with the CdSe/CdS core/shell nanocrystals with the lattice mismatch between core and shell of 3.9%, authors of[41] have observed the presence of a strain up to 50A. They have seen the obvious effect of strain, such as the peak shift toward larger d-spacing.

This supports our proposed model of thin layers with different lattice constant changing from core to shell. The authors of[41] noticed that "the strain in nanocrystals should involve a larger volume fraction than in a superlattice and have a correspondingly larger effect on a XRD patterns".

Chapter 4

QUANTUM DOT ARRAY IN AN ORGANIC HOST

In this Chapter, we present a theory for a new inorganic-organic hybrid exciton state, which appears when an array of semiconductor quantum dots is embedded in an organic medium. The hybrid exciton has uniques properties, which the Frenkel and Wannier-Mott excitons separately do not have, for example, it has both the large exciton radius and the large oscillator strength, and high non-linear optical susceptibility [42,43].

4.1 Introduction.

Development of innovative growth techniques such as molecular beam epitaxy and the realization of systems in two-, one- and zero-dimensional confined geometry made it possible to have many newly developed organic and

inorganic structures with very interesting properties[44,45]. The growth of organic multilayer structures analogous to semiconductor (inorganic) superlattices has been made in several groups[46-48]. This recent progress opens a new field of research for investigation of the optical properties of such systems, which is very promising from both the technological and the background scientific point of view. In particular, the possibilities of combining organic and inorganic materials in one heterostructure lead to a series of investigation of a new type of hybrid excitation in such systems[49-52].

In a solid, the excitons play an important and fundamental role in optical properties, especially for the optical processes happening close to or below the band gap. As said in Chapter 2, the exciton is a bound state of an electron and a hole, which is created by light. By Frenkel's definition, excitons are electron excitation waves which do not carry electric current. There are two different kinds of excitons in solids: the Frenkel excitons and the Wannier- Mott excitons. The Frenkel exciton is the electronic state of a molecular or strongly ionic crystal, where the electrons and the holes are situated on the same molecule or atom. The lattice constant of the molecular crystal is very small, $a \sim 5.4$, so the Frenkel exciton can be considered as a small radius exciton with $a_F \sim 5.4$. Another case is the Wannier-Mott exciton in the semiconductor. Within the effective mass approximation for the two -particle system with the Coulomb electron-hole interaction, the Wannier-Mott exciton can be represented by the hydrogen-like wavefunction.

The typical electron-hole distance is large, and the Wannier-Mott exciton is relatively weakly bound with the Bohr radii $a_B \sim 100A$ in III-V materials and $a_B \sim 30A$ in II-VI materials. So, the Frenkel excitons are also called the small radius excitons, while the Wannier Mott excitons are the large-radius excitons. Because of their large radius, the interaction between the Wannier-Mott excitons is very large, while the interaction between Frenkel exciton in different sites can be neglected in many cases. The Frenkel excitons have very strong oscillator strength, which is comparable to the oscillator strength of the molecule, while the oscillator strength of an Wannier-Mott exciton is much weaker.

The exciton resonance is reached when the exciton density equals the saturation density, i.e when the exciton wavefunctions begin to overlap each other. The small radii of the Frenkel excitons lead to their very large saturation density so that the excitonic resonance in organic material is very difficult to achieve due to too high concentration which is necessary. In constrast to that, the optical nonlinearity of the Wannier-Mott exciton can be large at rather low saturation density $n_s \sim 1/\pi a_B^2$ [52].

The differences between the Frenkel exciton of organic materials and the Wannier-Mott excitons of semiconductors gave scientists the idea to form the systems having some hybrid excitation states which has the composite properties of both kinds of excitons and in this way to overcome the limitation of each kind of excitons. Thus, one expects to have an hybrid exciton with

the large exciton radius of the Wannier exciton but possessing the large oscillator strength of the Frenkel exciton. Then the hybrid state can have at the same time the large optical resonance nonlinearity and the low exciton saturation density. By combining the organic and semiconducture in one heterostructure system, one expect to have the excitation state with all the major properties of both kinds of excitons.

To realize this idea, physicists propose systems with different geometrical configuration of organic-semiconductor materials[49-52] so that the Frenkel excitons of organic material and the Wannier-Mott excitons in semiconductor are in resonance of each other, and interact with each other by the dipole-dipole interaction at their interface to form the mixed state.

The very first effort in this field is the model of nanostructure consisting of a neighbouring organic quantum well and inorganic quantum well [49]. The resonant interaction of two kind of exciton at the interface of two 2D quantum wells leads to strong mixing and to the apperance of new states with the large exciton radii typical for Wannier-Mott excitons, and the large oscillator strength typical for the Frenkel excitons. The dispersion curves shifts the minimum away from the center of the Brillouin zone, which is expected to influence the optical properties. The dipole-dipole couling decays very fast with increasing the interwell distance. The new hybrid states exists in a large region of exciton wave vectors, but disappears in a range of small two-dimensional exciton wave vectors. Another configuration is proposed [50],

where the authors study the excited states in parallel neighboring organic and inorganic semiconductor quantum wires. For this geometry, the hybrid exciton state is different from zero even for zero wavevector. Recently, in [51] the interesting model of a single semiconductor quantum dot with an organic shell was also proposed and the strong mixing was found for the weak confinement regime in the limit of dot radius $R_D >> a_B$ (exciton Bohr-radius). For these models, the authors predict a large enhancement of nonlinearities at resonance, in some cases it is about two-orders of magnitude in comparison with the traditional systems.

As a new model for the heterostructures, where the resonant mixing of Wannier-Mott and Frenkel exciton can appear, we propose here the system of a semiconductor quantum dot array embedded in a medium of organic material. Such structures were reported to have been fabricated in several labs [47,48].

As was said in chapter 2, the oscillator strength of a quantum dot increases proportionally to the radius of the dot. So the optical non-linearities should also increase with increase of the dot radius as long as the quantum size effect of the zero-dimensional quantum dot still works. When the quantum dot radius is too large, the exciton energy becomes continuous as in the bulk semiconductor, the quantum size effect does not work any more, and the non-linearities stop increasing with the increasing of the dot's size. So, there is some size of the quantum dot, where the nonlinearities archieve the

maximum value, which is the limitation that the pure dot cannot overcome.

It is already known [54] that when many quantum dots are arranged together in an array, due to the multipole interaction of excitons in different dots, an exciton inside a quantum dot can be considered as not localized in that dot, but it can propagate through the lattice via the mechanism of exciton transfer processes. So, the quantum dot array can help to overcome the above limitation and can enhance the optical nonlinearities in the system.

When we place such a dot array in an organic material, due to the interaction of this propagating exciton with the medium, a new hybrid exciton state will appear in a system. This hybrid exciton, which is a mixed state of the transfer exciton and the Frenkel exciton of the medium when these are at resonance, also has a large exciton radius (because of the large Wannier-Mott exciton radius) and a large oscillator strength (because of the large oscillator strengths of the both Frenkel and transfer Wannier-Mott excitons). The small mass of the transfer exciton then leads to a large coherence length of the system. This fact, as well as the hybridization, will give us a very large optical non-linearity. It may also give unusual transport properties, but at the time of writing these have not been investigated.

In section 4.2 we present our model to get the hybrid exciton Hamiltonian. The hopping coefficient of the exciton in different dots and the Wannier-Frenkel exciton coupling constant are described in section 4.3 and 4.4. The nonlinear optical susceptibility and its dependence upon the system param-

eters are obtained in section 4.5, along with an estimate of the magnitude of the non-linear coefficient for a typical system.

4.2 The Model.

We consider a nanostructure consisting of a three dimensional array of semiconductor quantum dots placed into some organic material as a host medium. The size of the system should be considerably smaller than the wavelength of light that corresponds to the transition between excited and ground state [51]. As an approximation, we will consider here the ideal array with dots of the same radius R and the same dot-dot spacing d. The excitations in inorganic semiconductor quantum dots are the Wannier Mott excitons, which will interact with the Wannier-Mott excitons in other dots through the dipole-dipole interaction. The Frenkel exciton in the organic medium is represented as an electronic state of the crystal where the hole and the electron are situated at the same molecule.

The total Hamiltonian of the system will be taken as follows:

$$H = H_W + H_F + H_{int} \tag{4.1}$$

where H_W is the Wannier Mott exciton Hamiltonian, which consists of terms

for a free excitons and for the hopping between the excitons in different dots:

$$H_W = \sum_{\vec{n},l} E^W_{\vec{n}l}\, a^+_{\vec{n}l} a_{\vec{n}l} + \sum_{\vec{n}\vec{n}'ll'} t_{\vec{n}\vec{n}'ll'} (a^-_{\vec{n}l} a_{\vec{n}'l'} - h.c.) \qquad (4.2)$$

where $a^-_{\vec{n}l}$, $(a_{\vec{n}l})$ are creation (annihilation) operators of Wannier excitons in quantum dots. Index l labels the exciton states and $\vec{n}$ indicates the sites of the dot in the dot lattice. Here we assume that the dots are distributed on sites of a three-dimensional lattice with the position $\vec{n} = (n_x, n_y, n_z)$ of each site in (x,y,z) coordinates, where the distance between the sites (the "lattice" constant) equals d. For simplicity we assume a cubic array, i.e, the number of dots in each directions N_x, N_y, N_z is the same $N_x = N_y = N_z = N$.

The Frenkel exciton Hamiltonian can be written in the following form [49]:

$$H_F = \sum_{\vec{k},m} E^F_m(\vec{k}) b^-_{\vec{k}m} b_{\vec{k}m} \qquad (4.3)$$

where $b^-_{\vec{k}m}$, $(b_{\vec{k}m})$ are creation (annihilation) operators for the Frenkel exciton in the organic medium with wave vector $\vec{k}$ in the m^{th}-exciton state. Note here that because the Frenkel exciton is localized, the Frenkel exciton energy in the wavevector expansion 4.3 depends on k very weakly.

The interaction Hamiltonian between the Wannier Mott excitons in the dots and the Frenkel excitons in the medium has the form:

$$H_{int} = \sum_{nl\vec{n}\vec{k}} g_{lm}(\vec{r}_{\vec{n}}, \vec{k})(a^{+}_{\vec{n}l} b_{\vec{k}m}) \qquad (4.4)$$

In (4.2) and (4.3) $E^{W}_{\vec{n}l}$ and $E^{F}_{\vec{k}m}$ are the excitation energies of Wannier excitons in the dots and the Frenkel exciton in the host medium, respectively.

As was said in Chapter 2, for the Wannier excitons confined to a dot, or quantum sphere, the oscillator strengths are concentrated mainly on the low excited states. So, with no loss of generality, and in order to simplify we will consider only the interaction of the two lowest states of excitons(the ground state and the lowest excited state). Also we assume that the energy difference between the energy levels E^{F} and E^{W} is much smaller than the distance to other bands.

$g_{lm}(\vec{r}_{\vec{n}}, \vec{k})$ is the coupling constant of Wannier and Frenkel excitons, and $t_{\vec{n}\vec{n}'ll'}$ is the hopping constant between Wannier excitons in the dots. This hopping constant, which has its origin in the multipolar interaction of excitons in different dots, in general, is different in different directions because of the direction of polarization. Here we assume only nearest dots interact with each other, so the hopping constants for the nearest dots in the x, y, z direction are t_x, t_y, t_z, respectively, where e.g. $t_x = t_{\vec{n}\vec{n}'ll'}$ if $\vec{n}' = (n_x + 1, n_y, n_z)$

and l, l' are the label of the lowest energy levels, and similarly for t_y, t_z.

Because the dot radius is approximately equal to the ground state exciton Bohr radius for the systems under consideration, we assume there exists only one exciton in each dot, so we omit the exciton-exciton interaction in the same dot. Then we have for the hopping term:

$$H_{hop} = \sum_{ll'} \sum_{n_x,n_y,n_z} (t_x a^{+}_{n_x+1,n_y,n_z,l} a_{n_x,n_y,n_z,l'} + t_y a^{+}_{n_x,n_y+1,n_z,l} a_{n_x,n_y,n_z,l'} + t_z a^{+}_{n_x,n_y,n_z+1,l} a_{n_x,n_y,n_z,l'} + h.c.) \quad (4.5)$$

Changing to k-space by Fourier transformation with:

$$a^{+}_{n_x,n_y,n_z,l} = \frac{1}{\sqrt{N^3}} \sum_{k_x,k_y,k_z} [\exp i(n_x k_x d - n_y k_y d - n_z k_z d)] a^{+}_{k_x,k_y,k_z,l} \quad (4.6)$$

Here d is the distance between dots. $\vec{k} = \{k_x, k_y, k_z\}$ is the wave vector of the exciton in the coupled dots. The Fourier transform of t_x, t_y, t_z will be $t(k_x), t(k_y), t(k_z)$, respectively. Then we obtain the Hamiltonian for the Wannier- Mott exciton including the transfer exciton process in different dots:

$$H_W = \sum_{k,l} E_l^W(k) a_{kl}^+ a_{kl} + \sum_{k_x,k_y,k_z,l} [t(k_x)(e^{-ik_x a} + e^{ik_x a}) a_{kl}^+ a_{kl} +$$

$$+ t(k_y)(e^{-ik_y a} + e^{ik_y a}) a_{kl}^+ a_{kl} - t(k_z)(e^{-ik_z a} + e^{ik_z a}) a_{kl}^+ a_{kl}] \quad (4.7)$$

so we have:

$$H_W = \sum_{k,l} E_l^W(k) a_{kl}^+ a_{kl} + 2 \sum_l \sum_{k_x,k_y,k_z,l} [t(k_x) \cos k_x d -$$
$$+ t(k_y) \cos k_y d + t(k_z) \cos k_z d] a_{lk}^- a_{lk}^- \quad (4.8)$$

The Fourier transformation for the dot-medium coupling constant $g_{lm}(\vec{r}_{\vec{n}}, \vec{k})$ will be the following:

$$g_{lm}(\vec{r}_{\vec{n}}, \vec{k}) = \sum_{\vec{k}'} [\exp i(n_x k_x' d + n_y k_y' d - n_z k_z' d)] G_{lm}(\vec{k}', \vec{k}). \quad (4.9)$$

Notice here that if one makes the translational transformation with a lattice vector $\vec{L}$ in the lattice, due to the exponential forms of the Frenkel and Wannier exciton state functions, one will get, by translational invariance, $\sum_L \exp i(\vec{k} - \vec{k}')\vec{L} = \delta(k - k')$. So the coefficient $G_{lm}(\vec{k}, \vec{k}')$ will be different

from zero only if $k = k'$. Then instead of $G_{lm}(\vec{k}, \vec{k}')$ we can write the coupling constant as $G_{lm}(\vec{k})$ and omit the sum over k'.

Then we get the total Hamiltonian (4.1) as:

$$\begin{aligned} H &= \sum_{\vec{k}l} E^W_{ex}(\vec{k}, l) a^-_{l\vec{k}} a_{l\vec{k}} + \sum_{m\vec{k}} E^F_m(\vec{k}) b^-_{\vec{k}m} b_{\vec{k}m} \\ &+ \sum_{nl\vec{k}} G_{lm}(\vec{k})(a^-_{\vec{k}l} b_{\vec{k}m} + a_{\vec{k}l} b^-_{\vec{k}m}) \end{aligned} \tag{4.10}$$

where $E^W_{ex}(\vec{k}, l)$ is the energy of the Wannier-Mott exciton including the hopping transfer process as in (4.8).

In the perfect confinement approximation[1,2], the exciton wave functions must vanish at the boundary of dots, and the energy of the Wannier exciton in the spherical quantum dot has discrete values according to the zeros of the Bessel function. Then the energy of the Wannier exciton confined in the dot with quantum number $\{n, l\}$ is

$$E^W_{nl}(k) = E_g - E^b_{ext} - \frac{\hbar^2 \gamma^2_{nl}}{2M_{ex}R^2}, \tag{4.11}$$

where E_g is the band gap, E^b_{ext} is the exciton binding energy, and γ_{nl} is the n-th zero of the spherical Bessel function $j_l(x)$ of order l, which depends

on the magnitude of the dot radius R. Here M_{ex} is the effective mass of the exciton. The lowest excitation in the dot will be the state with $l = 0, n = 1$. As we consider only the lowest exciton state, from now on we will omit the index l of the exciton state. In writing the expression for $E^W_{nl}(k)$ we are assuming the dot is spherical as a good approximation to the actual shape.

For kd small, the total Hamilton (4.10) can be written as:

$$H = \sum_{\vec{k}} E^W_{tr}(\vec{k}) a^+_{\vec{k}} a_{\vec{k}} - \sum_{k} E^F(k) b^+_{\vec{k}} b_{\vec{k}} + \sum_{k} G(k)(a^+_{\vec{k}} b_{\vec{k}} + a_{\vec{k}} b^+_{\vec{k}}) \qquad (4.12)$$

Now we call $E^W_{tr}(\vec{k})$ the transfer energy of the Wannier exciton of the semiconductor dot array:

$$E^W_{tr}(\vec{k}) = E^W - 2\sum_i t(k_i) - d^2 \sum_i t(k_i) k_i^2, \qquad (4.13)$$

where $i = \{x, y, z\}$.

Equation (4.12) describes the system of Wannier excitons and Frenkel excitons, interacting with each other. Besides the exciton energy in single quantum dots, the energy of the Wannier exciton in the quantum dot array also includes the large transfer energy between two nearest quantum dots in the array.

We notice that because of confinement, the energy and the state of one quantum dot cannot be described by the wave vector. But the energy and the state of the transfer exciton in the quantum dot array does have the k-vector dependence and we will need to include the dispersion relation for the energy of this transfer exciton. This energy strongly depends on the value of the hopping constant $t(\vec{k})$ and the direction of the polarization vector of the exciton, which we will investigate in the next sections. The presence of the transfer exciton allows us to change the energy region of the resonance and also the optical properties of the hybrid exciton.

So in our model the semiconductor quantum dot array embedded in an organic medium can be interpreted as follows: the Wannier excitons in quantum dots interact with each other to form a kind of transfer exciton propagating through the lattice. This transfer exciton in its turn is coupled at resonance with the Frenkel excitons in the organic medium to form an hybrid organic-inorganic exciton state.

In our model we consider the exciton-exciton interaction and the hybridization as the principal effect, so here we omit the potential scattering between the dot array and the medium and leave it for future reseach.

4.3 The Hybrid Exciton State

We consider the case where the energy separation between the Wannier-Mott exciton and and the Frenkel excitons is much less than the distance to any other exciton band, and seek the mixed state only between the two nearest bands. As a basic set we choose the mixing state so that when the Wannier-Mott exciton is excited, the Frenkel exciton is in its ground state, and when the Frenkel exciton is excited, the Wannier-Mott exciton is in its ground state.

We write the new hybrid excited state as the following:

$$|\Psi(k)>= u_l(k) f^F(0) \Psi_l^W(k) + v_{l'}(k) f^W(0) |\Psi_{l'}^F(k)> \qquad (4.14)$$

where $\Psi^W(k)$ and $\Psi^F(k)$ are excited states and $f^W(0), f^F(0)$ are ground states of the Wannier exciton in the dot array and Frenkel excitons in medium, respectively. Since we will consider only the lowest excited states of the exciton, so from now on we will omit the indices l and l'. The coefficients u(k) and v(k) have the following form after making a Bogoliubov Transformation from operators a_k, a_k^+ and b_k, b_k^+ to new operators α_k, α_k^+ :

$$u(k) = \frac{G(k)}{\{[E^F(k) - E^W_{tr}(k)]^2 + G^2(k)\}^{1/2}}$$
$$v(k) = \frac{E^F(k) - E^W_{tr}(k)}{\{[E^F(k) - E^W_{tr}(k)]^2 + G^2(k)\}^{1/2}} \quad (4.15)$$

Then in term of hybrid operators $\alpha_{\vec{k}}, \alpha^+_{\vec{k}}$, the Hamiltonian in equation (4.12) can be written:

$$H' = \sum_k E(k)\alpha^+_{\vec{k}}\alpha_{\vec{k}} \quad (4.16)$$

with the energy $E(\vec{k})$ of the hybrid state given by the following dispersion relation:

$$E(\vec{k}) = 1/2\{E^F(\vec{k}) - E^W_{tr}(\vec{k})\} \pm 1/2\{[E^F(\vec{k}) - E^W_{tr}(\vec{k})]^2 + 4G^2(\vec{k})\}^{1/2} \quad (4.17)$$

Due to the weak dependence of the Frenkel exciton energy upon the k- vector, the Frenkel exciton energy may be taken independent of the wave vector k, $E^F(k) = E^F(0)$. We can see from (4.17) that the existence of the array of

dots, which results in the appearance of the transfer exciton energy $E_{tr}^{W}(\vec{k})$, enhances the coupling between these two kinds of exciton at resonance, i.e., the gap between two hybrid exciton branches becomes large. The coupling will be strong when $E^{F}(\vec{k})$ and $E_{tr}^{W}(\vec{k})$ are in resonance. So, the resonance coupling behavior depends strongly on the hopping coefficient $t(\vec{k})$ and the hybridization coefficient $G(\vec{k})$, which we will investigate in the next sections.

From (4.16) we can obtain the average exciton radius of the new hybrid exciton:

$$a_{hybrid} = |u(k)|^2 a_W - |v(k)|^2 a_F \tag{4.18}$$

where a_W, a_F are the radius of the Wannier-Mott exciton and Frenkel exciton, respectively. As we said, $a_W >> a_F$ and for strong hybrid state we have $a_{hybrid} \sim |u(k)|^2 a_W$. And since $u(k)$ depends on the coefficients G(k) and t(k), the hybrid exciton radius is also dependent on those coefficients.

4.4 Hopping coefficient $t(\vec{k})$

The hopping coefficient $t(\vec{k})$ is in fact the transfer energy between two nearest dots in the dot array and plays an important role in the processes occurring when a dot array is placed in an organic medium.

The transfer energy is estimated as the electrostatic interaction between excitons in dots [54]. Due to the existence of "confined" excitons, each dot has its transition dipole moment, which will interact with the corresponding moment of another dot when the distance between dots is comparable to the dot radius. As mentioned above, for one isolated quantum dot the oscillator strength is concentrated mainly on the lowest excited states and so we assume that only the transition dipole moment to the lowest excited states are involved in the interaction for an array. This multipolar interaction is intrinsically strongly short-range, and dependent upon the distance between dots,so we use here the nearest neighbor approximation.

Now consider the electrostatic interaction between excitons in two spherical quantum dots:

$$t(\vec{k}) = < W_i(\vec{k}) | H_{d-d} | W_j(\vec{k}) > \tag{4.19}$$

where $W_i(\vec{k}), W_j(\vec{k})$ are the exciton wave functions in two dots,

$$|W_i(\vec{k})> = \frac{1}{V_0}\int \phi(\vec{r}_i^{eh})\varphi(\vec{r}_i)e^{i\vec{k}(\vec{r}_{en}-\vec{r}_{hn})/2}\Psi_e^-(\vec{r}_{en})\Psi_h^-(\vec{r}_{hn})d\vec{r}_{en}d\vec{r}_{hn}|0> \tag{4.20}$$

where $\phi(\vec{r}_i^{eh})$ is the relative electron-hole motion function, $\vec{r}_i^{eh} = \vec{r}_{ei} - \vec{r}_{hi}$, $\varphi(\vec{r})$ is the exciton envelope function, $\vec{r}_{ei}, (\vec{r}_{hi}), \Psi_e^-(\vec{r}_{ei}), (\Psi_h^-(\vec{r}_{hi})$ are the coordinates and creation operators of electron (hole) in the dot, respectively. V_0 is the spherical dot's volume. The exponent e^{ikr} can be expressed in terms of spherical harmonics [58].

$$e^{-ikr} = 4\pi \sum_{ll'} \sum_{m,m'} (-i)^{l'} j_l(kr) Y_{l'm'} Y_{lm}$$

The envelope function for the exciton inside a spherical dot depends on the radius of the dot and has the form [1,4]:

$$\varphi(\vec{r}_i)_{nlm} = Y_{lm}(\theta_i, \phi_i) \frac{2^{1/2}}{R^{3/2}} \frac{j_{nl}(\gamma_{nl}\frac{r_i}{R})}{j_{n,l-1}(\gamma_{nl})} \tag{4.21}$$

where r_{eh} is the electron-hole relative coordinate and r is the center of mass coordinate of the exciton. H_{d-d} is the interaction Hamiltonian between two dipole moments in these two dots. In our case the distance between two dots is larger than the dot radius $d > R$, so the interaction can be considered approximately as the ordinary dipole-dipole interaction. But when the dot spacing is of the same order as of the dot radius, we have to consider the multipolar interaction. Neglecting the higher orders the interaction between two quantum dots can be written in the form:

$$H_{d-d} = \int \frac{3(\vec{r}.\vec{p}_2)(\vec{r}\vec{p}_1) + (\vec{p}_1.\vec{p}_2)r^2}{r^5} \tag{4.22}$$

where p_1, p_2 are the polarization vector of the Wannier Mott exciton in the two dots

$$p_i = \mu_D^W \Psi_e(r_e)_i \Psi_h(r_h)_i + h.c. \tag{4.23}$$

μ_D^W is the optical transition dipole moment of the Wannier-Mott exciton.

Put (4.22), (4.24) into (4.21), and then after some calculation we obtain for the hopping coefficient between two spherical quantum dots:

$$t(k) = \phi_{ns}(0)^2 f_{ns}\{(\vec{\mu}_1^w.\vec{\mu}_2^w) - 3(\vec{\mu}_1^w.\hat{n}_{12})(\vec{\mu}_2^w.\hat{n}_{12})\} \tag{4.24}$$

$\phi_{nl}(r)$ is the quantum dot exciton envelope function, $\vec{\mu}_{1,2}^w$ are transtion dipole moments to the excited state $(n, l = 0, m = 0)$ for the quantum dot spheres 1 and 2, respectively, $\hat{n}_{12}$ is the unit vector directed along the straight line connecting two excitons, which due to the small dot radius we can approximately treat as directed along the line connecting two dot centers. f_{ns} is the

integral:

$$f_{ns}(k) = \int j(kr)\varphi(\vec{r})_{ns} d^3r \int \frac{\varphi(\vec{r'})_{ns}}{|d + r - r'|^3} d^3r' \qquad (4.25)$$

The integrals are taken over the volume of the two dots.

For the exciton polarization parallel to the direction connecting two dot centers:

$$t_{\parallel} = -\phi_{ns}(0)^2 f_{ns} 2(\mu^{ex})^2 \qquad (4.26)$$

For the exciton polarization perpendicular to the direction connecting two dot centers the hopping coefficient is equal to:

$$t_{-} = \phi_{ns}(0)^2 f_{ns}(\mu^{ex})^2 \qquad (4.27)$$

The hopping constant depends strongly on the polarization direction of excitons. Also, the transfer energy (4.15) depends on the direction of k-vector and relationship between the k-vector and the polarization mode of the exciton. The longitudinal and transverse modes have different energies.

For the transition dipole moment to the excited state $(n, l = 0, m = 0)$ of the spherical quantum dot we have:

$$\mu^{cv} = \frac{(2)^{3/2}}{n\pi}\phi_{1s}(0)p_{cv}R^{3/2} \tag{4.28}$$

Hence, from (4.24) - (4.27), the hopping coefficient t depends on R/d, so we can change the dot separation d with respect to dot radius R in order to determine the optimum t for the strong hybridization state.

4.5 Hybridization parameter G(k)

The organic medium can also be described as a lattice, with organic molecules occupying every site. The Frenkel exciton can move between the sites. Because of the small "lattice constant" here, the organic molecular lattice can be considered as a "microscopic" lattice in comparison with the macroscopic size of the dot lattice. The organic "lattice constant" is of order 5Å, while the dot radius is about 30-100 Å and the dot lattice constant is usually around 60-500 Å. The resonance coupling of Frenkel excitons in the medium and Wannier excitons in the dot array is determined by the interaction parameter [49]:

$$G(k) = < F, k|H_{int}|W, k > \tag{4.29}$$

where the interaction Hamiltonian is taken similarly to [1, 3, 4]

$$H_{int} = -\sum_n E(r_n)P(r_n) \tag{4.30}$$

Here $E(r_n)$ is the operator of the electric field created at point r_n in the organic medium by the excitons in quantum dots, $P(r_n)$ is the transition polarization operator of the Frenkel exciton at molecular site r_n of the organic medium.

If the static dielectric constant of the semiconductor dots is ϵ_1, and of the organic medium is ϵ_2, the field at some point r_n outside of the dot, created by the exciton in the dot located at r is:

$$E(r - r_n) = \frac{3\epsilon_1}{2\epsilon_2 + \epsilon_1} \frac{3\hat{n}\cos\theta - \hat{\mu}}{(r - r_n)^3} \mu^D (\hat{a}^-_{nl}(r) + \hat{a}_{nl}(r)) \tag{4.31}$$

$P(r_n)$ is the polarization operator of the Frenkel exciton at molecular site r_n:

$$P(r_n) = \vec{\mu}^F (\hat{b}^-_n + \hat{b}_n) \tag{4.32}$$

$\vec{\mu}^F$ is the optical transition dipole moment of the organic molecule. The Frenkel exciton wave function is written in the form:

$$F(k) = \frac{1}{N_F^{1/2}} \sum_n e^{i\vec{k}\vec{r}_n} \chi_s^f(r_n) \hat{b}_n^+ |0> \tag{4.33}$$

$\varphi_s(r_n)$ is the excited state of the molecule at site r_n. Putting (4.32) - (4.35) into (4.31), we have the expression for the hybridization coefficient of the semiconductor quantum dot and the organic medium

$$G(k) = \frac{3\epsilon_1}{2\epsilon_2 + \epsilon_1} \frac{\tau}{2} \frac{\sin\theta}{(N^F)^{1/2}} \mu^F \mu^w \phi_{ns}(0) D_{ns}(k) \tag{4.34}$$

where θ is the angle between exciton transition dipole moments of the quantum dot and the organic molecule, and

$$D_{ns}(k) = \int_{Medium} e^{i\vec{k}\vec{r}'} \chi_{ns}^f(r') d^3r' \int_{Dot} \frac{\varphi_{nlm}(r)}{r'|r - r'|^3} d^3r \tag{4.35}$$

The first integral is taken over the dot and the second one is taken over the volume of the whole medium.

For illustration a numerical calculation was done for some samples. Fig. 4.2 shows the hybrid exciton dispersion curves plotted for ZnSe dots embedded in a standard organic material. The parameters were taken as $a_B = 30\mathring{A}, \mu^F = 5D, N = 5$. In Fig 4.1 two branches of the hybrid exciton are plotted for an array of dots with radius $R = 40\mathring{A}$, and the dot lattice constant $d = 80\mathring{A}$.

4.6 Non - Linear Optical Response

In the presence of the external electric field

$$E(r) = E_0 e^{i\vec{q}\cdot\vec{r}} \tag{4.36}$$

the interaction Hamiltonian of the electric field with the hybrid exciton is described in the following form:

$$H_{int} = E_0 \left[\int_{Medium} p^F(r) e^{i\vec{q}\cdot\vec{r}} - \int_{Dot} p^W(r) e^{i\vec{q}\cdot\vec{r}} \right] dr \tag{4.37}$$

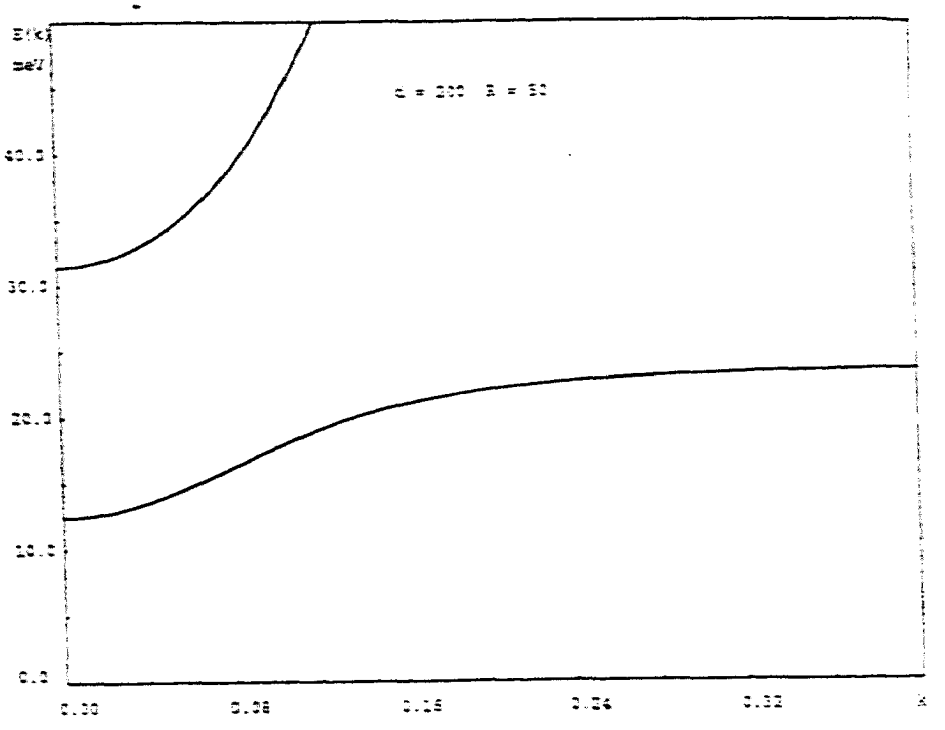

Figure 4.1: *Hybrid Exciton Dispersion calculated for ZnSe dots placed in an organic material The dispersion curve is ploted for dot radius* $R = 50\text{Å}$ *and dot spacing* $d = 200\text{Å}$

The matrix element consists of two parts: the Wannier Mott exciton matrix element and the Frenkel exciton matrix element:

$$< \alpha, k|\hat{H}_{int}|0 >= E_0[u(k)M^F + v(k)M^W] \tag{4.38}$$

where M^F and M^W is the optical matrix element of the Frenkel exciton and Wannier exciton, respectively. In the region of mixing, the oscillator strength of the hybrid exciton is determined as:

$$f(\vec{k}) = |u(\vec{k})|^2 f^F + |v(\vec{k})|^2 f^W \tag{4.39}$$

Both components, the transfer Wannier and the Frenkel exciton, give contributions to the oscillator strength of the hybrid exciton. Due to the confinement effect of the exciton in one single dot as well as the transfer exciton coupling between dots in the array, the Wannier transfer exciton oscillator strength may achieve a value comparable to that of the Frenkel exciton, which is very big due to their small exciton radius and small molecular lattice constant. So, placing of many semiconductor dots in an organic medium leads to a large oscillator strength of the hybrid exciton. At resonance, the

oscillator strength of the hybrid state is determined by its Frenkel exciton component.

From the above result, we see the hybrid exciton has both the large exciton radius and large oscillator strength. The large radius leads to rather low saturation density, and so we have at the same time the large oscillator strength and the low saturation density, which promise the large nonlinearities of the state.

As already noted in [53] and can be seen from (4.15), the Wannier transfer exciton has a rather small translational mass, which depends on the hopping constant and the number of dots. For instant, for the simple case where we assume all $t_x = t_y = t_z = t$, comparing the (4.15) with the energy formula $E = \hbar^2 k^2/2m$, we have the formula for the so called translational mass

$$M = \frac{\hbar^2}{2t^2 d^2} \tag{4.40}$$

This translational mass depends on the hopping constant between dots and the dot-dot spacing, and it will be a few times smaller than the ordinary reduced electron-hole mass.

This small translational mass is one reason for a large coherence length, which is related to the homogeneous linewidth of the excitonic transition[54].

$$l_c = \left(\frac{3\pi^2}{2^{1/2}}\right)^{1/3} \frac{\hbar}{(M\hbar\Gamma_h)^{1/2}} \tag{4.41}$$

M is the exciton translational mass (4.42) which we can control by changing the system parameters namely dot radius and dot spacing. Γ_h is the linewidth of the exciton V is the volume of the whole system, V_{Medium} is the volume of the organic host, and V_{cell} is the volume of one cell in the organic lattice. Notice here that we consider the case where the sample size is smaller than the coherence length, so the size dependence appears as in (29).

In the presence of an electric field, the third-order susceptibility can be calculated using standard pertubation theory [56-60]. By definition the third-order non-linear optical polarization of an exciton is written as:

$$< P^{(3)}(r,t) > = \left(\frac{-i}{\hbar}\right)^3 \int_{-\infty}^{t} dt_1 \int_{-\infty}^{t_2} dt_2 \int_{-\infty}^{t_2} dt_3 < P(r,t)[H'(t_1),$$

$$[H'(t_2),[H'(t_3),\rho_0]]] > \qquad (4.42)$$

Each term in the above integral consists of the contribution from intermediate states, which can be one-exciton states or two-exciton states. In the vicinity of an exciton resonance, however, it is found [53] that the magnitude of $\chi^{(3)}$ can be safely approximated by the contribution from one-exciton states only and can be approximately computed as:

$$Im\chi^{(3)} = \frac{1}{V}\sum_{i}\left(\frac{e^2}{2m_0\omega_i}\right)^2 \frac{f_{X_i}^2}{(\omega-\bar{\omega}+i\gamma_\perp)^2(\omega-\bar{\omega}-i\gamma_\parallel)} \qquad (4.43)$$

where V is the system volume, $\gamma_\perp, \gamma_\parallel$ are the longitudinal and transverse relaxation rate, $\hbar\bar{\omega}$ is the lowest excitation energy of the hybrid exciton. f_{X_i} is the exciton oscillator strength. The summation is taken over all the exciton levels lying within the homogeneous linewidth of the ground exciton state. The oscillator strength is determined by the coherence volume (4.43), which is related to the homogeneous linewidth, which reflects the energy fluctuation of the exciton state. So, the oscillator strength of the k=0 exciton state is redistributed among all states within the homogeneous linewidth and is written as:

$$f_X = f_0(l_c)^3|\phi(0)|^2 \qquad (4.44)$$

where f_0 is the oscillator strength (4.41)of the band-to-band transition, and $\phi(0)$ is the envelope function of the exciton.

Considering only the resonance case and neglecting contributions from the other nonresonant levels and taking into account (4.41)-(4.46) we have approximately the result for the optical nonlinearity of the hybrid excitons:

$$\chi^{(3)}(\omega) \approx \frac{\mu_F^4}{V}\frac{(2\sqrt{2})^4}{\pi^2}\left(\frac{V_{Medium}}{V_{cell}}\right)^2 l_c^3\left(\frac{R}{d}\right)^6 \phi_{1s}^4(0)\left[\frac{1}{(\omega-\tilde{\omega}+i\gamma_\perp)^2(\omega-\tilde{\omega}-i\gamma_\parallel)}\right] \tag{4.45}$$

V_{Medium} is the volume of the organic host, and V_{cell} is the volume of one cell in the organic lattice. The result (4.45) includes the contribution from the lowest exciton state.

The value of $\chi^{(3)}(\omega)$ in (28) at resonance may be very large. By changing the number of dots and other parameters of the array, one can control value of the non-linearity.

Also, we have to note here one more factor for the optical non-linearities. The figure of merit of the exciton is defined as the relative change $\Delta\chi/\chi$ of nonlinear susceptibility in the presence of a pump density I_p. And the relationship between the figure of merit and the saturation density and the coherence length can be written as the following:

$$\frac{\sigma}{\alpha_0} \sim 2(l_c)^3 \sim \frac{N}{N_s} \tag{4.46}$$

So, the increase of the coherence length leads to a large figure of merit of the exciton, and, associated with it, low saturation density, large exciton

resonance oscillator strength and the large non-linearity [53].

4.7 Illustrative Calculations

Here we present some numerical results for ZnSe dots.

In Fig. 4.2 the third-order nonlinear susceptibility of ZnSe quantum dot lattice embedded in an organic material is plotted for several different dot radii and dot spacings. We use here the following typical parameters of organic and semiconductor materials: $v^F = 100\dot{A}, a_{org} = 5\dot{A}, \mu^F = 5D, a_{1B} = 30\dot{A}, E^F(0) - E^W(0) = 5meV$. We see that at resonance, e.g. where the hybridization is strongest, we have very high peak of nonlinear susceptibility with the enhancement of about 5 orders of magnitude in comparison with that of the Wannier exciton. The nonlinear coefficient is larger for smaller dots and closer spacing between them. Also we expect that disorder in the semiconductor dot array will decrease the enhancement effect, but this required a separate investigation which has not been carried out yet.

4.8 Summary

We presented in this chapter the possibility of creating systems which offer a strong resonance coupling of Frenkel and Wannier excitons to obtain an hybrid exciton state with the special properties of both kinds of exciton.

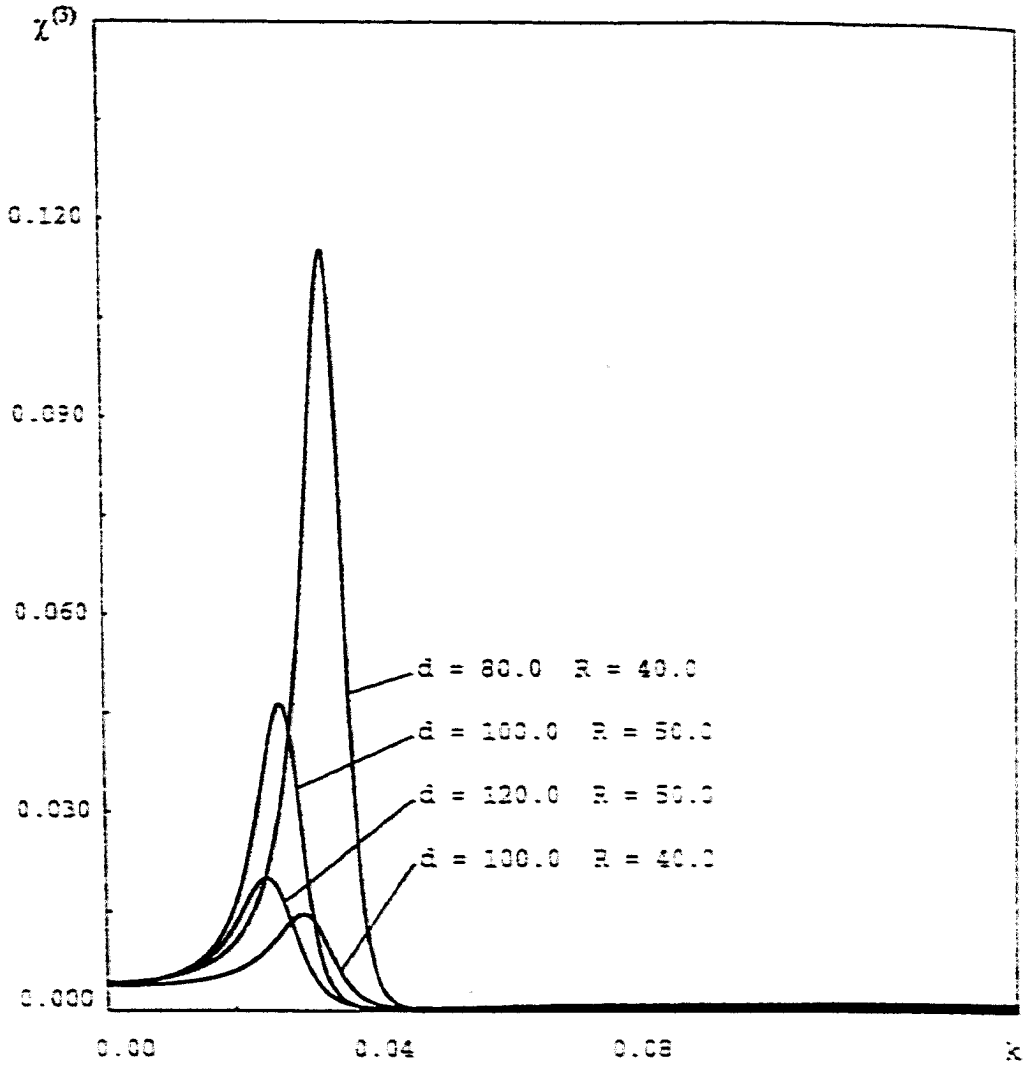

Figure 4.2: *Third-order nonlinear susceptibility for the hybrid exciton state of ZnSe dots in organic material. We plot the susceptibility versus wave - vector. Note that there is a very significant enhancement of* $\chi^{(3)}$. *Plots are for different dot radius R and separation d*

i.e.having large exciton radius as well as large oscillator strength. In addition, we can control the expected resonance parameters by changing the number of dots, their radius, the distance between them, and the dot radius and dot separation ratio.

Chapter 5

MANGANESE-DOPED NANOCRYSTALS

In this chapter we will present our study of Mn-doped nanocrystals ZnS. We will consider the effect of an extra electron in the doped quantum dot $ZnS:Mn^{2+}$. The effect of Coulomb interaction and exchange interaction between the extra electron and the states of the Mn ion will mix the wavefunctions, split the impurity energy levels and break the previous selection rules and change the transition probabilities. Using this model of an extra electron in the doped quantum dot, we calculate the energy and the wave functions, the luminescence efficiency and the transition lifetime and compare with the experiments.

5.1 Introduction

In contrast to undoped materials, the impurity states in doped nanocrystal plays an important role in the electronic structure, transition probabilities and the optical properties. An attempt to understand more about these zero-dimensional nanocrystals efforts has been made in several labs[61-71] by doping an impurity in a nanocrystal and searching for a novel material and properties. When the size of the nanocrystals is reduced to the size comparable to some characteristic lengths, such as the effective Bohr radius around the impurity center or the electronic de Broglie wavelength, the effect of the confinement effect on the energy states and wavefunctions of the impurity will occur, and unusual physical and optical properties are expected to be found.

In recent years, Mn-doped ZnS nanoparticles have been intensively studied. Among many wide band gap compounds, manganese is well known as an activator for photoluminescence (PL) and electroluminescence (EL) and the Mn^{2+} ion d-electrons states act as efficient luminescent centers while doped into a semiconductor. In order to find the way to improve the efficiency, people are trying to reduce the size of the doped nanocrystal.

In 1994 Bhargava and Gallagher[61, 62] reported the first realization of ZnS semiconductor nanocrystal doped with Mn isoelectronic impurities and claimed that Mn-doped ZnS nanocrystal can yield both the high lumines-

cence efficiency and lifetime shortening. The doped nanocrystals ZnS:Mn were prepared by an organometalic reaction at room temperature and these nanocrystals were coated with polymer or monomer to maintain the separation of the particles. The report claimed that their EXAFS experiments confirm that the Mn^{2+} ion was occupying the site of Zn^{2+} ion. In this system the authors [61, 62] observed the significant increase of the quantum efficiency when the system was exposed to the 300 nm UV light. For the ZnS:Mn nanocrystals, when exposed to the exciting 300 nm UV light, the room temperature quantum efficiency increases gradually but rather significantly with the decreasing size of the nanocrystals, from $< 1\%$ for the nanocrystal of radius 70 Åto 18% for the nanocrystal of radius 35 Å. In Fig (5.1) the size dependence of the quantum efficiency is shown[62]. The spectra of nanocrystal were measured under identical conditions, so the ratio of the PL intensities reflects the ratio of their luminescence efficiency.

The yellow emission characterrized for Mn^{2+} in bulk ZnS [77], which is associated with the transition $^4T_1 - ^6_1$, was claimed to be observed in photoluminescence (PL) spectra for the Mn^{2+} in nanocrystal ZnS. In nanocrystals, however, the PL peak for the yellow emission is reported slightly shifted toward a lower energy (in bulk ZnS:Mn it peaks arount 2.12 ev, in nanocrystal ZnS:Mn it peaks at 2.10 eV). Also, the linewidth of the yellow emision in the PL spectrum for nanocrystal is larger than for the bulk. In Fig (5.2) the PL spectra for nanocrystals of different radii are shown to compare with the PL

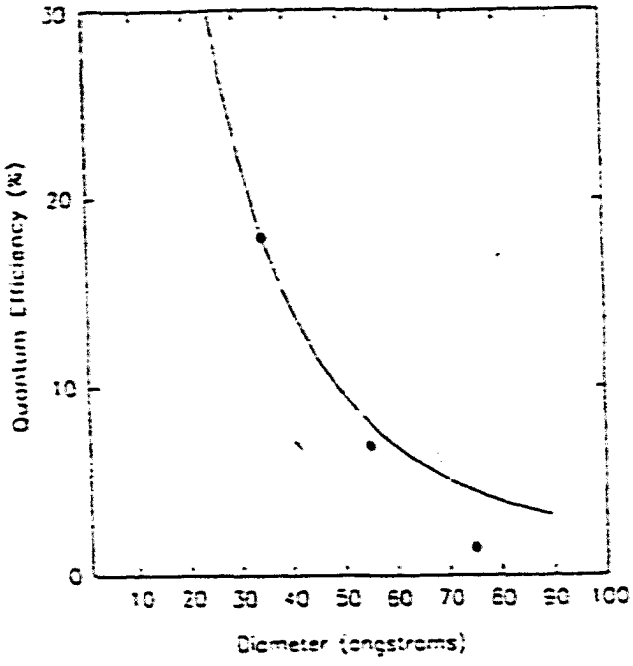

Figure 5.1: *Variation of the luminescence efficiency as a function of the size of the nanocrystals*

spectra of the bulk.

The luminescence lifetime of the Mn^{2+} $^4T_1 - ^6A_1$ transition was reported to decrease by 5 orders of magnitude, from 1.8 ms in bulk to 3.7 ns and 20.5 ns in nanocrystals while maintaining the high (18%) quantum efficiency.

The authors[66] suggested that the increase in quantum efficiency as well as the lifetime shortening is the result of strong hybridization of s-p electrons of the ZnS host and d- electrons of the Mn impurity due to confinement, and also of the modification of crystal field near the surface of the nanocrystals.

Stimulated by this dramatic result, many other laboratories are trying to synthesize the Mn-doped ZnS nanocrystals and considerable attention has

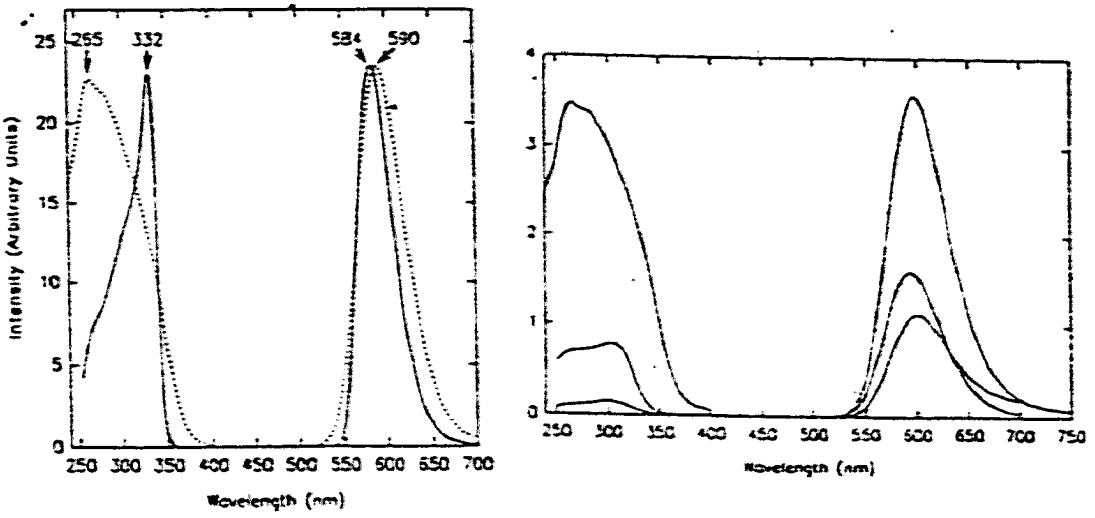

Figure 5.2: *The PLE and PL spectra of bulk (dashed line) and of nanocrystals of various sizes (solid lines)*

been paid to optical properties of these kind of materials[67-74]. The papers of Yu et al. [71] reports to obtain the yellow characteristic emission peak of ${}^4T_1 - {}^6A_1$ and the peak is slightly shifted toward the higher energy. Also, they obtain the increase in the luminescence efficiency of the nanocrystal ZnS:Mn in comparison with the bulk Mn-doped ZnS. Sooklal et al.[69] reported the shortening of the decay time to ns for nanocrystal $ZnS : Mn^{2+}$ while Ito et al. [70] obtained the life time shortening to μs in $ZnTe : Mn^{2+}$ quantum well. Also, several different workers have proposed models to try to explain the processes happening with the impurity centers inside the confined nanocrystals [73, 75]. But if it is now well established that the confinement

effect strongly modified the electronic structure of nanocrystals, the effects of the Mn-impurity on the electronic structure of the nanocrystal, or to put in a different way, the effects of the confinement on the energy structure and transitions of the Mn impurity in the nanocrystals, still are controversial. In fact, there is still no settled mechanism to explain the changes in optical properties of the Mn in the nanocrystals. Also, if some labs reports that they also obtained the large change in optical properties of ZnS:Mn nanocrystals, there are some other reports claiming no change in the luminescence results in comparison with the Mn-doped semiconductor bulk [72,74].

Tanaka et al [72] studied the ZnS:Mn nanocrystal and found the quantum efficiency of the ZnS:Mn nanocrystal higher than the Mn-doped ZnS bulk. But they also found that the local structure around the Mn^{2+} ion remain similar to the bulk, and does not depend on the size of the nanocrystals, so they conclude that the confinement does not increase the mixing of sp-electrons of the host and d-electrons of the Mn^{2+} ion and the sp-d mixing is not responsible for the enhancement of the photoluminescence efficiency.

In addition, in [74], Bol and Meijerink showed that the luminescence of the ZnS:Mn nanocrystal have actually two kinds of decay time, one short ($\sim 100ns$), and one long ($\sim 1.9ms$ - which is typical for the bulk doped ZnS:Mn). And also, they argued that the short decay time is not from the decay of ${}^4T_1 - {}^6A_1$ at all, but is associated with the defect-related emission of ZnS. And they conclude that the doped semiconductor nanoparticles do

not form a new kind of material.

The aim of our work in this chapter is to study more about the doped ZnS:Mn nanocrystals. We consider a new mechanism for the Mn doped ZnS nanocrystal, namely the effect of an extra electron in the doped nanocrystal, and consider what mechanism will then occur, to affect the electronic structure and optical properties of the nanocrystals.

5.2 Model of an Injected Extra Electron in a Nanocrystal

Here we propose a new mechanism to control the emission and other optical transitions in a nanocrystal. Our model is to inject an extra electron into the quantum dot. The extra electron will strongly couple to the electron involved in the transitions, split energy levels and mix the wavefunctions, and will thus strongly break the former selection rules. Because the dot is small, the boundary conditions make the coupling very strong, so by controling the presence or absence of the extra electron in the dot, one can control the optical transitions in the dot. This can provide the explanation to the observed shortening lifetime and enhancement of the quantum efficiency.

The transition of our interest here is ${}^4T_1 - {}^6A_1$ of the Mn^{2+} ion in the crystal field of the ZnS nanocrystal. The luminescent transition from the lowest excited level ${}^4T_1$ (spin $\frac{3}{2}$) to the ground state (spin $\frac{5}{2}$) is spin-forbidden.

But, the weak spin-orbital interaction makes the transition slightly allowed [75,77,78].

If an extra electron is in the dot, the electron will couple with the electrons of Mn^{2+} in each state, namely the electron will couple with the states $^4T_1$ and $^6A_1$. In this work we consider as the coupling hamiltonian the exchange interaction. The wavefunctions of the d^5 electrons in $^6A_1$ and $^4T_1$ states will be derived in the next two sections. For the extra electron which is confined in the dot, we will use the wavefunction for confined electron in the sphere:

$$\varphi_(^{D\alpha}1s) = R_{1s}^{D\alpha} Y_0^0 |\frac{1}{2}, \sigma > \tag{5.1}$$

where Y_0^0 is a spherical harmonics, $|\frac{1}{2}, \sigma >$ is spin function for the electron with spin $s = \frac{1}{2}$ and $\sigma = +$ or - for spin up and spin down states. $R_{1s}^{D\alpha}$ is the envelope function for the electron confined in a sphere of radius R (2.4)

$$R_{nl}^{D\alpha} = \sqrt{\frac{2}{R^3}} \frac{j_l(\chi_{nl}\frac{r}{R})}{j_{l+1}(\chi_{nl})} \tag{5.2}$$

where j_{nl} is the spherical Bessel function, χ_{nl} is the zero of the spherical Bessel function.

The interaction Hamiltonian between the extra electron and the d^5 elec-

trons is given in section 5. In section 3 we will recall the strong field limit approximation for a single d electron in a crystal field, so that section 4 we can derive the wavefunctions for the d^5 electrons in $^4T_1$ and $^6A_1$ states.

5.3 A Single 3d Electron in the Crystal Field-Strong Coupling Limit

Impurity centers are formed by foreign ions substituting for host ions or placed interstitially in the lattice. When the activator ions such as Mn are placed in the crystal field of the semiconductor lattice, the crystal field would affect the wavefunctions and energy structure of the impurity to form so called crystal field states of the impurity ions. For the transition metal ions with the outer $3d^n$ electron configuration, the crystal field energy and the interelectron Coulomb interaction are comparable[78,79], so these d^n electrons can be treated in the intermediate crystal field or in the strong crystal field limit, and they are more often treated in the strong field approximation. In the next section we will present the application of strong crystal field approximation for the case of $3d^5$ electrons of Mn^{2+} ions. To do that, at first in this section we recall some well known results for a single 3d electron. We consider an ion having a single 3d electron outside the closed shell placed in an octahedral crystal field. In terms of spherical harmonics, the octahedral crystal field Hamiltonian can be expressed as the following [79]:

$$H_c^{O_h}(r) = \frac{Ze^2}{4\pi\epsilon_0}\left[\frac{6}{a} + \frac{7r^4}{2a^5}\left\{C_0^{(4)}(\theta,\phi) + (\frac{5}{14})^{1/2}(C_4^{(4)}(\theta,\phi) + C_{-4}^{(4)}(\theta,\phi)\right\}\right] + r^6 terms + ... \tag{5.3}$$

where $\vec{r}(r,\theta,\phi)$ is the position of the d-electron,

$$C_t^{(k)}(\theta,\phi) = (\frac{4\pi}{2k+1})^{1/2} Y_k^t(\theta,\phi), \tag{5.4}$$

Y_k^t is the spherical harmonic. The values of the integrals over angles, $c^k(l'm_{l'}, lm_l) = < Y_{l'}^{m_l'} | C_t^{(k)} | Y_l^{m_l} >$ are given in the Table 5.1, with some conditions for non-zero value:

$$\begin{aligned} t &= m_l' - m_l, \\ k - l + l' &= \text{eveninteger}, \\ |l - l'| &< k < l + l' \end{aligned} \tag{5.5}$$

To evaluate the effect of $H_c^{O_h}$ on the 3d electron states, we have to evaluate the matrix elements of the type:

$$< n'l'm_l'|r^k C_t^{(k)}|nlm_l >=< R'_{n'l'}|r^k|R'_{nl} > \left\langle Y_{l'}^{m_l'} \left| C_t^{(k)} \right| Y_l^{m_l} \right\rangle \qquad (5.6)$$

The radial integral can cause configuration mixing, but because of the large separation between the energies of d the mixing can be ignored and it is assumed that nl=n'l'. Then the matrix elements of $H_c^{O_h}$ will remain inside the states of the 3d configuration. The nonzero matrix elements will be the following [79]:

$$\begin{aligned}
< 3d0|H_c^{O_h}|3d0 > &= 6Dq \\
< 3d1|H_C^{O_h}|3d1 > &= < 3d-1|H_c^{O_h}|3d-1 >= -4Dq \\
< 3d2|H_c^{O_h}|3d2 > &= < 3d-2|H_c^{O_h}|3d-2 >= Dq \\
< 3d2|H_c^{O_h}|3d-2 > &= < 3d-2|H_c^{O_h}|3d2 >= 5Dq
\end{aligned} \qquad (5.7)$$

where we employ conventional notation as:

$$D = \frac{1}{4\pi\epsilon_0}\frac{35Ze^2}{4a^5}, \qquad q = \frac{2}{105} < r^4 >_{3d} \qquad (5.8)$$

Then we have the Hamiltonian matrix

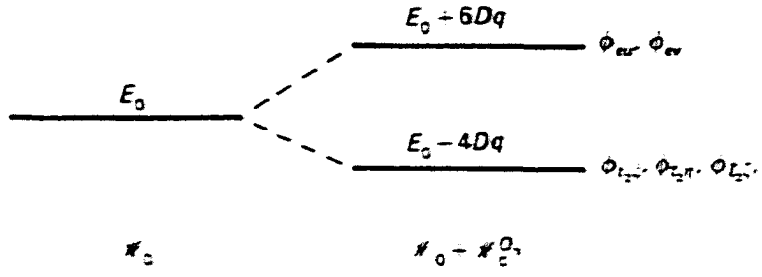

Figure 5.3: *Splitting diagram of a single 3d electron in the octahedral crystal field. The five-fold degenerate d-electron with energy E_0 splits in an octahedral crystal field into two levels with the separation of 10 Dq.*

$$\begin{bmatrix} Dq & 0 & 0 & 0 & 5Dq \\ 0 & -4Dq & 0 & 0 & 0 \\ 0 & 0 & 6Dq & 0 & 0 \\ 0 & 0 & 0 & -4Dq & 0 \\ 5Dq & 0 & 0 & 0 & Dq \end{bmatrix} \tag{5.9}$$

that can be diagonalized to obtain eigenstates and eigenvalues. Then the fivefold degenerate 3d level will split into two levels, the two-fold degenerate level with the additional energy $-6Dq$, and the three-fold degenerate one with the additional energy of $-4Dq$. In Fig. 5.3 the splitting diagram for a 3d electron in the octahedral crystal field is shown [79].

The eigenstates of the two-fold degenerate level (the e-orbitals) are written in the following form:

$$\begin{aligned}
\phi_{eu} &= |3d0>= R'_{3d}(r)(\frac{5}{4\pi})^{1/2}(\frac{3z^2-r^2}{2r^2}), \\
\phi_{ev} &= (\frac{1}{2})^{1/2}(|3d2>+|3d-2>) = R'_{3d}(r)(\frac{5}{4\pi})^{1/2}3^{1/2}(\frac{x^2-y^2}{2r^2}) \quad (5.10)
\end{aligned}$$

And the eigenstates for the three-fold degenerate level (the t_2-orbital) are written as:

$$\begin{aligned}
\phi_{t_2\xi} &= (\frac{i}{2})^{1/2}(|3d1>+|3d-1>) = R'_{3d}(r)(\frac{5}{4\pi})^{1/2}3^{1/2}(\frac{yz}{r^2}), \\
\phi_{t_2\eta} &= -(\frac{1}{2})^{1/2}(|3d1>-|3d-1>) = R'_{3d}(r)(\frac{5}{4\pi})^{1/2}3^{1/2}(\frac{xz}{r^2}), \\
\phi_{t_2\zeta} &= -(\frac{i}{2})^{1/2}(|3d2>-|3d-2>) = R'_{3d}(r)(\frac{5}{4\pi})^{1/2}3^{1/2}(\frac{xy}{2r^2}) \quad (5.11)
\end{aligned}$$

For simplicity, from now on we will denote these double degenerate and triple degenerate eigenstates u, v, ξ, η and ζ, respectively.

The calculation of $3d^m$ electron states in the crystal field is much more complicated than in the case of a single electron. In the next section, we will derive the wavefunctions of the $3d^5$ electrons with help of the symmetry of the crystal field.

5.4 $3d^5$ Electron in the Crystal Field - Crystal Field Manganese Energy Levels and Wavefunctions

For a multi-3d-electron system, the orbital Hamiltonian in crystal field will be the following:

$$H = \sum_i H_0^0(r_i) + \sum_{i>j} H'(r_i, r_j) \tag{5.12}$$

where $H_0^0(r_i)$ is the Hamiltonian (5.1) of single electron interacting with crystal field in the previous section, $H'(r_i, r_j)$ is the electron- electron interaction Hamiltonian between the d-electrons. For the strong crystal field limit, the Hamiltonian $H_0^0(r_i)$ will be solved of first to obtain the wavefunctions of a single 3d electron as in the last chapter, then these states will be interacting by the Hamiltonian $H'(r_i, r_j)$ The wavefunctions of 3d-electron orbitals are u, v, which belong to the E irreducible (in O_h) representation, and ξ, η, ζ which belong to the T_2 reducible representation. So in the strong crystal field case, the wavefunctions of multi-3d-electron Hamiltonian will be the products of these one-electron orbitals.

In an octahedral crystal field, the Hamiltonian (5.9) is invariant under all the rotation operators of the group O, where for the first term of (5.9),

the rotations are applied independently for each r_i and for the second term, the rotations are applied simultaneously for all r_i Then the wavefunctions will transform according to irreducible representation of the O group. The products of irreducible representations of the group O follow the following rules

$$
\begin{aligned}
A_1 \times A_1 &= A_1, & E \times E &= A_1 + A_2 + E, \\
A_1 \times A_2 &= A_2, & E \times T_1 &= T_1 + T_2, \\
A_1 \times E &= E, & E \times T_2 &= T_1 + T_2, \\
A_1 \times T_1 &= T_1, & T_1 \times T_2 &= A_2 + E + T_1 + T_2, \\
A_1 \times T_2 &= T_2, & T_1 \times T_1 &= A_1 + E + T_1 + T_2, \\
A_2 \times A_2 &= A_1, & T_2 \times T_2 &= A_1 + E + T_1 + T_2, \\
A_2 \times E &= E, \\
A_2 \times T_1 &= T_2, \\
A_2 \times T_2 &= T_1,
\end{aligned}
\tag{5.13}
$$

where A_1, A_2 are one-dimensional representations (A_1 is symmetric and A_2 is antisymmetric), E is the two-dimensional representation and T_1, T_2 are

three-dimensional representations of the group O.

Begining the reduction process for the two 3d electrons configuration, we will have the products $E \times E, T_2 \times T_2$ and $T_2 \times T_2$. The $E \times E$ product functions will belong to A_1, A_2 and E irreducible representation. From table (5.1) for Clebsch-Gordan coefficients, the product functions of the $E \times E$ orbitals will be:

$$\begin{aligned} |e^2, A_1> &= \frac{1}{\sqrt{2}}[u(r_1)u(r_2) + v(r_1)v(r_2)] \\ |e^2, A_2> &= \frac{1}{\sqrt{2}}[u(r_1)v(r_2) - v(r_1)u(r_2)] \\ |e^2, Eu> &= \frac{1}{\sqrt{2}}[u(r_1)u(r_2) - v(r_1)v(r_2)] \\ |e^2, A_1> &= \frac{1}{\sqrt{2}}[u(r_1)v(r_2) + v(r_1)u(r_2)] \end{aligned} \tag{5.14}$$

The $|e^2, A_1>$ function is symmetric under interchange of r_1, r_2. Then because of the Pauli principle, to obtain the antisymmetric function its spin function must be the antisymmetric spin function with the total spin S=0

$$|S = 0, M_S = 0> = \frac{1}{\sqrt{2}}[\alpha(\sigma_1)\beta(\sigma_2) - \beta(\sigma_1)\alpha(\sigma_2)] \tag{5.15}$$

where $\alpha(\sigma)$ and $\beta(\sigma)$ are the up ($|\uparrow>$) and down ($|\downarrow>$) spin functions.

And the full wavefunction $|e^2, A_1>$ will be the product of the orbital and the spin function:

$$|e^2, A_1, M_S = 0 >= \frac{1}{2}[u(r_1)u(r_2) + v(r_1)v(r_2)][\alpha(\sigma_1)\beta(\sigma_2) - \beta(\sigma_1)\alpha(\sigma_2)] \tag{5.16}$$

Using the notation for the Slater determinant:

$$[u^- u^-] = \frac{1}{\sqrt{2}} \begin{vmatrix} u(r_1)\alpha(\sigma_1) & u(r_2)\alpha(\sigma_2) \\ u(r_1)\beta(\sigma_1) & u(r_2)\beta(\sigma_2) \end{vmatrix} \tag{5.17}$$

the final full wavefunction $|e^2, A_1>$ is written in the short form

$$|e^2, A_1, M_S = 0 >= \frac{1}{\sqrt{2}}\left([u^- u^-] - [v^+ v^-]\right) \tag{5.18}$$

Similarly for the wavefunctions $|e^2, A_2>$ of the $E \times E$ orbitals we have the antisymmetric orbital wavefunction, then the spin functions must be three symmetric spin functions of the total spin S=1:

$$|S = 1, M_S = 1> \; = \; \alpha(\sigma_1)\alpha(\sigma_2)$$

$$
\begin{aligned}
|S=1, M_S=0> &= \frac{1}{\sqrt{2}}[\alpha(\sigma_1)\beta(\sigma_2)+\beta(\sigma_1)\alpha(\sigma_2)] \\
|S=1, M_S=-1> &= \beta(\sigma_1)\beta(\sigma_2)
\end{aligned}
\tag{5.19}
$$

Then the total wavefunctions of $|e^2, A_2>$ will have the form:

$$
\begin{aligned}
|e^2,{}^3A_2, M_S=1> &= |u^- v^-| \\
|e^2,{}^3A_2, M_S=0> &= \left([u^- v^-]+[u^- v^-]\right) \\
|e^2,{}^3A_2, M_S=-1> &= [u^- v^-]
\end{aligned}
\tag{5.20}
$$

Similarly for the $|e^2, E>$ wavefunctions

$$
\begin{aligned}
|e^2,{}^1Eu, M_S=0> &= \frac{1}{\sqrt{2}}\left([u^- u^-]-[v^- v^-]\right) \\
|e^2,{}^1Ev, M_S=0> &= \frac{1}{\sqrt{2}}\left([u^- v^-]-[u^- v^-]\right)
\end{aligned}
\tag{5.21}
$$

In the same way for the $T_2 \times T_2$ [79]:

$$
|t_2^2,{}^1A_1> = \frac{1}{\sqrt{3}}\left([\xi^+\xi^-]+[\eta^-\eta^-]+[\zeta^+\zeta^-]\right)
$$

$$
\begin{aligned}
|t_2^{2\,1}Eu> &= \frac{1}{\sqrt{6}}\left(-[\xi^+\xi^-]-[\eta^+\eta^-]+2[\zeta^+\zeta^-]\right)\\
|t_2^{2\,1}Ev> &= \frac{2}{\sqrt{3}}\left([\xi^+\xi^-]-[\eta^+\eta^-]\right)\\
|t_2^{2\,1}T_2,\xi> &= \frac{1}{\sqrt{2}}\left([\eta^+\zeta^-]-[\eta^-\zeta^+]\right)\\
|t_2^{2\,1}T_2,\eta> &= \frac{1}{\sqrt{2}}\left([\zeta^-\xi^+]-[\zeta^+\xi^-]\right)\\
|t_2^{2\,1}T_2,\zeta> &= \frac{1}{\sqrt{2}}\left([\xi^+\eta^-]-[\xi^-\eta^+]\right)\\
|t_2^{2\,3}T_1\alpha, M_S=1> &= \frac{1}{\sqrt{3}}[\eta^-\zeta^-]
\end{aligned}
\tag{5.22}
$$

and for t_2e configuration:

$$
\begin{aligned}
|t_2e,^1T_1\gamma> &= \left([\zeta^-v^-]-[\zeta^-v^+]\right)\\
|t_2e,^3T_1\gamma, M_S=1> &= [\zeta^-v^-]\\
|t_2e,^1T_2\zeta> &= \frac{1}{\sqrt{2}}\left([\zeta^-u^-]-[\zeta^-u^+]\right)\\
|t_2e,^1T_1\gamma> &= [\zeta^-u^+]
\end{aligned}
\tag{5.23}
$$

Continuing in this way one can get all the possible wavefunctions and energies for t^n, e^n and $t^m e^k$ configuration of $3d^n$ in the octahedral crystal field

[80]. The functions of t^m and e^n are given in the Appendix 1 [80]. In Fig.(5.4) is the energy diagram for d^5 configuration calculated by Tanabe and Sugano [80].

The ground state of the $3d^5$ configuration is the sextet $^6A_1$ with the total spin $\frac{1}{5}$. The first excited level is the triplet states $^4T_1$, which is the excited state closest to the ground state. We are interested in the optical transition between the first excited state and the ground state, this is the transition $^4T_1 - ^6A_1$. The wavefunctions of the states $^6A_1$ and $^4T_1$ can be calculated. The wavefunction of $^6A_1$ and $^4T_1$ states can be derived, using the table of coupling coefficients from [80,82].

The ground state - the sextet $^6A_1$ is derived from $t_2^3 \times e^2$. From the table (5.2) the $^6A_1$ state is:

$$\begin{aligned} |^6A_1> &= \left|t_2^3(^4A_2)e^2(^3A_2), ^6A_1a_1\right\rangle \\ &= \left|t_2^3(^4A_2)\right\rangle \left|e^2(^3A_2)\right\rangle \end{aligned} \tag{5.24}$$

The function of $t_2^3(^4A_2)$ and $E^2(^3A_2)$ are (Appendix 1)

$$\begin{aligned} |t_2^3(^4A_2)\frac{3}{2}a_2> &= [-\xi^+\eta^-\zeta^-] \\ |e^2(^3A_2)1a_2> &= [u^+v^-] \end{aligned} \tag{5.25}$$

134 *Symmetry and Group Representation Theory*

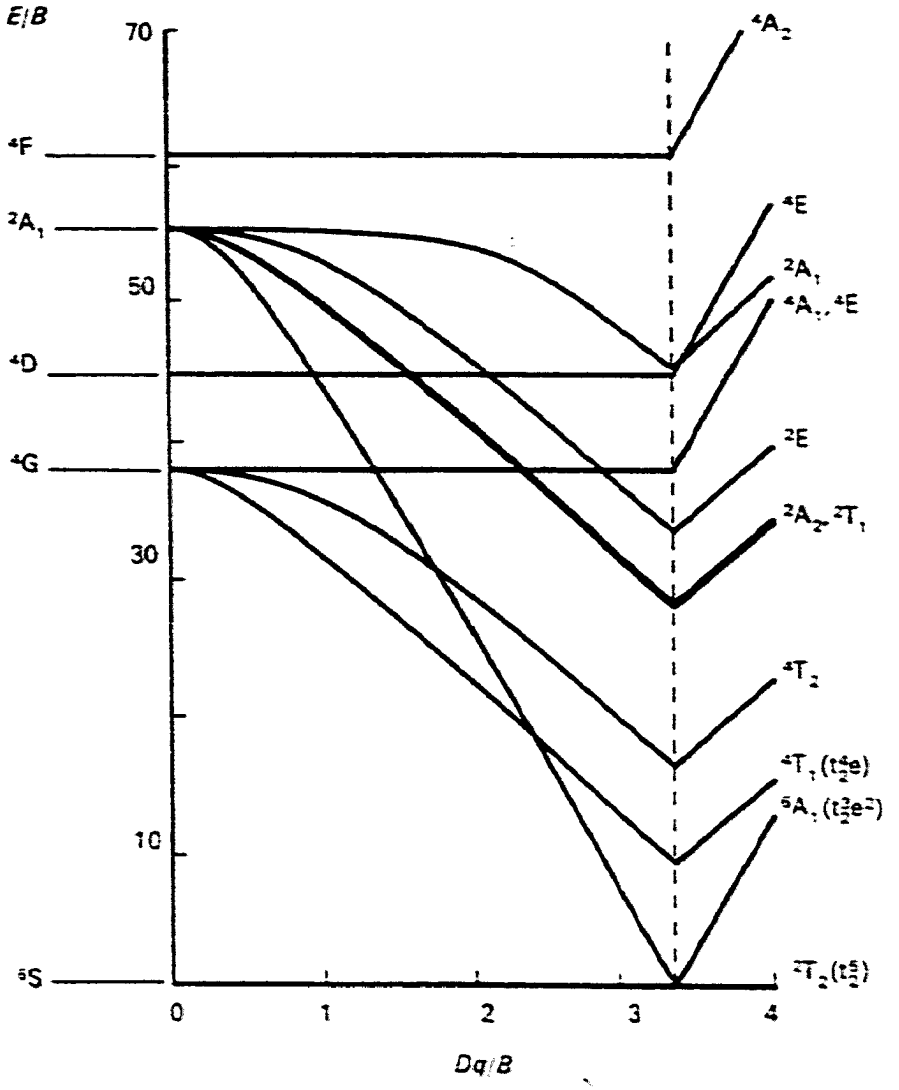

Figure 5.4: *Energy digram for d^5 electrons in the octahedral crystal field*

Then we have for the wavefunctions of the ground state ${}^6A_1$:

$$|{}^6A_1 a_1 >= |-\xi^- \eta^+ \zeta^- u^+ v^-| \tag{5.26}$$

$A_2 \times A_2$		A_1
		a_1
a_2	a_2	1

Table 5.1. The coupling coefficients of $A_2 \times A_2$ representations

The triplet ${}^4T_2$ wavefunctions of $3d^5$ are derived from $t_2^4({}^3T_1) \times e^1({}^2E)$.

$$\begin{aligned}
|{}^4T_1 \frac{3}{2} z > &= t_2^4({}^3T_1) e^1({}^2E), {}^4T_2 \frac{3}{2} z > \\
|{}^4T_1 \frac{3}{2} y > &= t_2^4({}^3T_1) e^1({}^2E), {}^4T_2 \frac{3}{2} y > \\
|{}^4T_1 \frac{3}{2} z > &= t_2^4({}^3T_1) e^1({}^2E), {}^4T_2 \frac{3}{2} z >
\end{aligned} \tag{5.27}$$

The functions of $t_2^4({}^3T_1), x, y, z >$ are (Appendix 1):

$$
\begin{aligned}
|t_2^4(^3T_1)1y> &= -[\xi\eta^-\eta^-\zeta^-] \\
|t_2^4(^3T_1)1z> &= [\xi^-\eta^-\zeta^-\zeta^-]
\end{aligned}
\tag{5.28}
$$

From the table (5.2) we have the wavefunctions of the triplet $^4T_1$ of the $3d^5$ configuration:

$$
\begin{aligned}
|^4T_1\frac{3}{2}x> &= -\frac{1}{2}|t_2^4(^3T_1)1x, e^1(^2E)u> + \frac{\sqrt{3}}{2}|t_2^4(^3T_1)1x, e^1(^2E)v> \\
|^4T_1\frac{3}{2}y> &= -\frac{1}{2}|t_2^4(^3T_1)1y, e^1(^2E)u> + \frac{\sqrt{3}}{2}|t_2^4(^3T_1)1y, e^1(^2E)v> \\
|^4T_1\frac{3}{2}z> &= |t_2^4(^3T_1)1z, e^1(^2E)u>
\end{aligned}
\tag{5.29}
$$

$E\times T_1$		T_1			T_2		
		x	y	z	ξ	η	ζ
θ	x	$-\frac{1}{2}$	.	.	$-\frac{1}{2}\sqrt{3}$	.	.
θ	y	.	$-\frac{1}{2}$	.	.	$\frac{1}{2}\sqrt{3}$	.
θ	z	.	.	1	.	.	.
ϵ	x	$\frac{1}{2}\sqrt{3}$	.	.	$-\frac{1}{2}$	.	.
ϵ	y	.	$-\frac{1}{2}\sqrt{3}$	.	.	$-\frac{1}{2}$	.
ϵ	z	.	.	.	.	.	1

Table (5.2). The coupling coefficients of $E \times T_1$ representations.

And finally we have for the wavefunctions of the triplet $^4T_1$ of the d^5 configuration in the octahedral crystal field:

$$
\begin{aligned}
|^4T_1\frac{3}{2}x> &= -\frac{1}{2}[\xi^+\xi^-\eta^+\zeta^+u^+] - \frac{\sqrt{3}}{2}[\xi^-\xi^-\eta^+\zeta^+v^+] \\
|^4T_1\frac{3}{2}y> &= \frac{1}{2}[\xi^+\eta^+\eta^-\zeta^+u^+] + \frac{\sqrt{3}}{2}[\xi^+\eta^+\eta^-\zeta^+v^+] \\
|^4T_1\frac{3}{2}z> &= [\xi^+\eta^+\zeta^+\zeta^-u^+]
\end{aligned} \tag{5.30}
$$

We recall here that the wavefunctions in (5.24) and (5.28) are Slater determinants which we have written in the short notation. For demonstration we write here the full form of one of the functions

$$
[\xi^+\eta^+\zeta^+\zeta^-u^+] = \frac{1}{\sqrt{5}}\begin{vmatrix}
\xi(r_1)\alpha(\sigma_1) & \ldots & \xi(r_5)\alpha(\sigma_5) \\
\eta(r_1)\alpha(\sigma_1) & \ldots & \eta(r_5)\alpha(\sigma_5) \\
\zeta(r_1)\alpha(\sigma_1) & \ldots & \zeta(r_5)\alpha(\sigma_5) \\
\zeta(r_1)\beta(\sigma_1) & \ldots & \zeta(r_5)\beta(\sigma_5) \\
u(r_1)\alpha(\sigma_1) & \ldots & u(r_5)\alpha(\sigma_5)
\end{vmatrix} \tag{5.31}
$$

5.5 The Exchange Interaction

The exchange interaction will couple the extra electron and the d^5 electrons to have different spin configurations, so we expect this will make the spin-forbidden transition become allowable. The exchange interaction between the extra electron and the d^5 configuration has the following form:

$$
H_{ex} = -jS_{Mn}s_e \tag{5.32}
$$

where S_{Mn} is the total spin of the d^5 configuration in the states of interest, s_e is spin of the injected electron. j is the exchange matrix element, which has the form:

$$j_{ik} = \sum_{k,\lambda} < \bar{\phi}_k \bar{\phi}_\lambda | V | \phi_\lambda \phi_k > \tag{5.33}$$

where ϕ_k is the electron wavefunction, V is the two-electron interaction operator:

$$V(r_1, r_2) = \frac{q_1 q_2}{r_{12}} \tag{5.34}$$

Because both the wavefunctions of the extra electron (5.1) and of the d^5 electrons in the $^6A_1$ and $^4T_1$ state (5.26), (5.30) are expressed in terms of spherical harmonics, it will be natural that for the two-electron interacting operator V we want to use the expression in terms of the spherical harmonics. V can be expanded in the form[80]:

$$V(r_1, r_2) = \frac{q_1 q_2}{r_>} \sum_{k=0}^{\infty} \frac{r_<^k}{r_>^k} P_k(cos\theta) \tag{5.35}$$

where the $P_k(cos\theta)$ are the Legendre polynomials and can be expanded in term of spherical harmonics by the spherical harmonic addition theorem:

$$P_l(cos\theta) = \frac{4\pi}{2l-1} \sum_{m=-l}^{m=+l} Y_{lm}(1)\overline{Y}_{lm}(2) \tag{5.36}$$

Then:

$$V(r_1, r_2) = \frac{q_1 q_2}{r_>} \sum_{k=0}^{\infty} \frac{4\pi}{2k+1} \frac{r_<^k}{r_>^k} \sum_m Y_{km}(1)\overline{Y}_{km}(2) \tag{5.37}$$

If we put the electron functions into the equations (5.3) and (5.4), the matrix elements will consist of two parts - the radial part and the angular part:

$$< \phi_i\phi_j|V|\phi_m\phi_t >= \sum_{k=0}^{\infty} \rho^k(n^i l^i, n^j l^j, n^m l^m, n^t l^t) \times A_k \sigma(s^i s^t)\sigma(s^j s^m) \tag{5.38}$$

where $\rho^k(n^i l^i, n^j l^j, n^m l^m, n^i m^t)$ is the radial part

$$\rho^k(n^i l^i, n^j l^j, n^m l^m, n^t m^t) = < R_{n^i l^i} R_{n^j l^j} | \frac{e^2 r_<^k}{r_>^{k-1}} | R_{n^m l^m} R_{n^t l^t} > \qquad (5.39)$$

and A_k is the angular part

$$A_k = \frac{4\pi}{2k+1} \sum_{p=-k}^{+k} (\overline{Y}_{l^i p^i} Y_{kp} Y_{l^t p^t}) (\overline{Y}_{l^j p^j} \overline{Y}_{kp} Y_{l^m p^m}) \qquad (5.40)$$

where $(\overline{Y}_{l^i p^i} Y_{kp} Y_{l^t p^t})$ is a Clebsch-Gordan coefficient, which is different from zero only when the following conditions are satisfied:

$$\begin{aligned} p^i &= p + p^t \\ k + l^i - l^t &= \text{even} \\ l^i - l^t &\leq l^i - l^t \end{aligned} \qquad (5.41)$$

These conditions will reduce the terms in the sum (5.40) and leave only several matrix elements different from zero.

Now with the wavefunctions (5.1), (5.26), (5.30) and the exchange interaction (5.33), (5.37) we are ready to calculate the exchange interaction

between the extra electron and the electrons in d^5 configuration.

5.6 Exchange Interaction of Mn^{2+} Ion with the Extra Electron in the Nanocrystal

Now we suppose that the extra electron inside the nanocrystal is close enough to the Mn^{2+} ion at the center so that the electron can couple via exchange interaction with the d^5 electrons in both the ground state ${}^6A_1$ and the excited state ${}^4T_1$.

The matrix element of the exchange interaction of the injected electron and the d^5 electrons in the ${}^6A_1$ state:

$$\left\langle {}^6A_1(\vec{r})\varphi_{1s}^{D\alpha}(\vec{r'})|V(r-r')|\varphi_{1s}^{D\alpha}(\vec{r}){}^6A_1(\vec{r'})\right\rangle$$

$$= \left\langle \overline{[-\xi^+\eta^+\zeta^+u^-v^+]}(r)\overline{R_{1s}^{D\alpha}(r')Y_0^0}\,|V(r-r')|\,R_{1s}^{D\alpha}(r)Y_0^0[-\xi^-\eta^-\zeta^-u^-v^-](r)\right\rangle \tag{5.42}$$

We should pay attention here to the point that the wavefunction of the ${}^6A_1$ state of d^5 electrons is a Slater determinant with five single d-electron wavefunction. So the coordinate $\vec{r}$ of the d^5 electron wavefunction is actu-

ally five different coordinates $(r_1, r_2, r_3, r_4, r_5)$ of these five single d-electron wavefunctions (see 5.31). In fact, the extra electron has an exchange interaction with each of the five d-electrons. Because these five coordinates are independent, the integrals will be taken separately.

In the calculation of the determinantal matrix elements of (5.42), we have to deal with the single electron matrix element of the type, for example:

$$\langle \xi(r)\varphi(r')|V(r-r')|\varphi(r)\xi(r')\rangle$$

$$= \frac{4\pi q_1 q_2}{j_1(\pi)^2}\frac{1}{R^3}\sum_{k=0}^{\infty}\frac{1}{2k+1}\left\langle \overline{R_{3d}(r)}\left(\overline{Y_2^1}+\overline{Y_2^{-1}}\right)\overline{j_0}\left(\pi\frac{r'}{R}\right)\overline{Y_0^0}\right| \times$$

$$\left.\frac{r^k}{r'^{k+1}}\sum_{m=-k}^{k}Y_k^m(1)Y_k^m(2)\right| j_0\left(\pi\frac{r}{R}\right)Y_0^0 R_{3d}(r')\left(Y_2^1+Y_2^{-1}\right)\Big\rangle \quad (5.43)$$

or,

$$\langle \xi(r)\varphi(r')|V(r-r')|\varphi(r)\xi(r')\rangle$$

$$= \frac{4\pi q_1 q_2}{j_1(\pi)^2}\frac{1}{R^3}\sum_{k=0}^{\infty}\frac{1}{2k+1}\left\langle \overline{R_{3d}(r)}\overline{j_0}\left(\pi\frac{r'}{R}\right)\right| \frac{r^k}{r'^{k-1}}\left| j_0\left(\pi\frac{r}{R}\right)R_{3d}(r')\right\rangle$$

$$\times\left[\left\langle \overline{Y_2^1 Y_0^0}\right|\sum_{m=-k}^{k}Y_k^m(1)\overline{Y_k^m}(2)\left|Y_0^0 Y_2^1\right\rangle\right.$$

$$+\left\langle \overline{Y_2^1 Y_0^0} \left| \sum_{m=-k}^{k} Y_k^m(1)\overline{Y_k^m}(2) \right| Y_0^0 Y_2^{-1} \right\rangle$$

$$+\left\langle \overline{Y_2^{-1} Y_0^0} \left| \sum_{m=-k}^{k} Y_k^m(1)\overline{Y_k^m}(2) \right| Y_0^0 Y_2^{1} \right\rangle$$

$$+\left\langle \overline{Y_2^{-1} Y_0^0} \left| \sum_{m=-k}^{k} Y_k^m(1)\overline{Y_k^m}(2) \right| Y_0^0 Y_2^{-1} \right\rangle \Bigg] \qquad (5.44)$$

The conditions (5.41) for non-zero Clebsch-Gordan coefficients give the selection rules for k and m. Because of the selection rules, it is less difficult in calculation of the angular part, also it determines the terms of the sum in the radial part. Here k can be only 2. And the radial part of the matrix element becomes:

$$\rho(3d, s, k=2) = \int r^2 dr \int r'^2 dr' \frac{r^2}{r'^3} R_{3d}(r) R_{3d}(r') R_{10}^{Dot}(r) R_{10}^{Dot}(r') \qquad (5.45)$$

Here $R_{10}^{Dot}(r)$ is the envelope function (5.2) for the electron confined in a dot. R_{3d} is the orbital function of the 3d-electron, which can be approximately taken as Slater function[80] $R_{3d}(r) = r^2 e^{-1.87r/a}$, where $a = \frac{\hbar^2}{me^2}$ The first integral is taken over the Mn-ion radius (assuming that the Mn - ion is

situated at the center of the dot), the second integral is taken over the dot size. Then the radial integral $\rho(3d, s, k = 2)$ (5.45) can be computed and the matrix element (5.43) has the form:

$$\langle \xi(r)\varphi(r')|V(r-r')|\varphi(r)\xi(r')\rangle = \frac{2q_1q_2}{j_1(\pi)^2R^3}\rho(3d, s, k = 2) \qquad (5.46)$$

As the result of the calculation for determinantal matrix element (5.42), we receive the exchange matrix element (5.33) for the d^5 electrons and the extra electron:

$$j(^6A_1, \varphi_{1s}^{D\alpha}) = 10\frac{q_1q_2}{j_1(\pi)^2R^3}\rho(3d, s, k = 2) \qquad (5.47)$$

and for the exchange matrix elements of the d^5 electrons in $^4T_1$ states:

$$\begin{aligned} j(^4T_1z, \varphi_{1s}^{D\alpha}) &= 10\frac{q_1q_2}{j_1(\pi)^2R^3}\rho(3d, s, k = 2) \\ j(^4T_1x, \varphi_{1s}^{D\alpha}) &= 2(5+2\sqrt{3})\frac{q_1q_2}{j_1(\pi)^2R^3}\rho(3d, s, k = 2) \\ &= j(^4T_1y, \varphi_{1s}^{D\alpha}) \end{aligned} \qquad (5.48)$$

And as the effect of the exchange interaction (5.32) with the injected electron, the levels ${}^6A_1$ will be shifted and split into 2 sublevels with total spin $S = 3$ and $S = 2$ with the corresponding exchange energy:

$$\begin{aligned} E_{ex}({}^6A_1, \varphi(1s,+), S=3) &= -\frac{5}{4} \times 10 \frac{q_1 q_2}{j_1(\pi)^2 R^3} \rho(3d, s, k=2) \\ E_{ex}({}^6A_1, \varphi(1s,-), S=2) &= \frac{7}{4} \times 10 \frac{q_1 q_2}{j_1(\pi)^2 R^3} \rho(3d, s, k=2) \end{aligned} \tag{5.49}$$

with the corresponding wavefunctions:

$$\begin{aligned} |{}^6A_1, \varphi(1s,+), S=3> &= [-\xi^- \eta^+ \zeta^- u^+ v^-]|s+> \\ |{}^6A_1, \varphi(1s,+), S=2> &= [-\xi^+ \eta^- \zeta^- u^+ v^-]|s-> \end{aligned} \tag{5.50}$$

And the ${}^4T_1$ levels splits into four sublevels: two sublevels with the value of the total spin $S = 2$:

$$E_{ex}(^4T_1, z\varphi(1s,+), S=2) = -\frac{3}{4}\times 10\frac{q_1q_2}{j_1(\pi)^2R^3}\rho(3d,s,k=2)$$

$$E_{ex}(^4T_1, xy\varphi(1s,+), S=2) = -\frac{3}{4}\times 2(5+2\sqrt{3})\frac{q_1q_2}{j_1(\pi)^2R^3}\rho(3d,s,k=2) \quad (5.51)$$

and the two sublevels with the total spin $S=1$

$$E_{ex}(^4T_1, z\varphi(1s,-), S=1) = \frac{5}{4}\times 10\frac{q_1q_2}{j_1(\pi)^2R^3}\rho(3d,s,k=2)$$

$$E_{ex}(^4T_1, xy\varphi(1s,+), S=2) = \frac{5}{4}\times 2(5+2\sqrt{3})\frac{q_1q_2}{j_1(\pi)^2R^3}\rho(3d,s,k=2) \quad (5.52)$$

with the corresponding wavefunctions:

$$|^4T_1 z, \varphi(1s,+), S=2> = [\xi^-\eta^-\zeta^-\zeta^-u^-]s-> $$

$$|^4T_1xy,\varphi(1s,+),S=2> = \frac{\sqrt{2}}{2}[\xi^+\xi^-\eta^+\zeta^+u^+]|1s+) + \frac{\sqrt{6}}{2}[\xi^+\xi^-\eta^+\zeta^+v^+]|1s+>$$

$$-\frac{\sqrt{2}}{2}[\xi^-\eta^+\eta^-\zeta^+u^+]|1s+> + \frac{\sqrt{6}}{2}[\xi^+\eta^+\eta^-\zeta^+v^+])|1s+> \tag{5.53}$$

and

$$|^4T_1z,\varphi(1s,-),S=1> = [\xi^-\eta^-\zeta^+\zeta^-u^+]|s-> \tag{5.54}$$

$$|^4T_1xy,\varphi(1s,-),S=1> = \frac{\sqrt{2}}{2}[\xi^-\xi^-\eta^+\zeta^-u^+]|1s-> + \frac{\sqrt{6}}{2}[\xi^-\xi^-\eta^+\zeta^-v^+]|1s->$$

$$-\frac{\sqrt{2}}{2}[\xi^-\eta^+\eta^-\zeta^-u^+]|1s-> + \frac{\sqrt{6}}{2}[\xi^-\eta^+\eta^-\zeta^+v^+]0|1s->$$

The two sublevels $|^4T_1z,\varphi(1s+),S=2)$ and $|^4T_1xy,\varphi(1s+),S=2>$ of the $^4T_1$ state of the Mn^{2+} ion and the sublevel $|^6A_1,\varphi(1s-),S=2>$ now have the same total spin $S=2$ and the transition between them now are allowable. In Fig. (5.5) is the exchange energy splitting of the $^4T_1$ and $^6A_1$ levels and the transitions allowable between them.

So the exchange interaction between the electron injected in the dot and the d- electrons of the Mn-impurity center really make the previously forbidden transition become allowable. In the next section we will give some numerical calculations for the transition probability and the transition life-

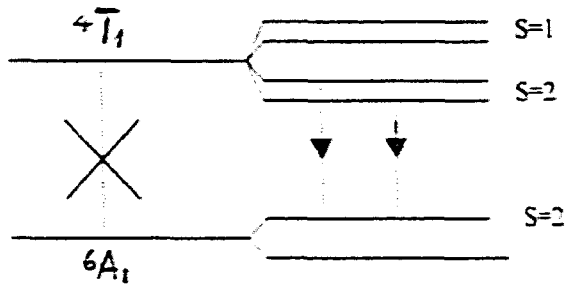

Figure 5.5: *Exchange energy splitting of the $^4T_1$ and $^6A_1$ states of the Mn^{2-} ion. Arrows indicate the allowable transitions*

time.

5.7 Luminescence and the Lifetime of the Transition

The electric dipole transition matrix element between two state $k >$ and $s >$ is written in the form[82]:

$$< k|r.\hat{e}|s >= \frac{4}{3}\sum_q \left\langle k \left| r.Y_1^q\left(\frac{\vec{r}}{r}\right) \right| s \right\rangle \times Y_1^{-q}\left(\frac{\vec{e}}{e}\right) \qquad (5.55)$$

So the matrix element of the transition between the sublevels of the state $^4T_1$ and $^6A_1$ will again have the form of the determinantant matrix element

between the wavefunctions (5.55) and (5.50) of the Mn-ion and the extra electron, respectively. Again, here we can separate the radial and the angular part

$$\left\langle {}^{4}T_1 zz, \varphi_{1s+}^{Dot}, S = 2 \left| r.\dot{e} \right|^6 A_1, \varphi_{1s-}^{Dot} \right\rangle$$

$$= \left\langle \overline{\left[\xi^- \eta^+ \zeta^- \zeta^- u^+ \right] < s+ \left| r \right| \left[-\xi^- \eta^- \zeta^- u^- v^+ \right]} \left| s- > \right. \right\rangle$$

$$= \left\langle R_{3d} R_{1s}^{Dot} \left| r \right| R_{3d} R_{1s}^{Dot} \right\rangle \left\langle (i) \, Y_1^{-q} \, (j) \right\rangle \tag{5.56}$$

where $< (i)|r|(j) >$ denote the angular part and the $< |r| >$ – the radial part. Similar to the calculation of the exchange matrix element in the last section, the angular part is calculated using the Clebsch-Gordan coefficients. The radial part also can be computed. Note here that the radial part of the exchange interaction matrix element, in general, is difficult to calculate. But for the case of a nanocrystal, when we use the envelope function as the Bessel function, the integral becomes easier to compute when using the expansion of the zero-order Bessel function.

And for the radial function of d-electron of Mn ion we use the approximate expression [80]

$$R_{3d} \sim r^2 e^{-1.87r/a} \tag{5.57}$$

with $a = \hbar^2/me^2$. Then the integral can be computed approximately.

We now do numerical calculations for the case of a quantum dot of Mn-doping ZnS of radius 50Å. We use here the standard parameters of Mn and ZnS. For this doping ZnS:Mn quantum dot, we obtain the exchange coefficient $j \sim 0.1eV$, splitting due to exchange will be 1.0 to 1.5 eV, which is rather large. The probability of the transition approximately equals $5.4 \times 10^4 s^{-1}$ It results in a lifetime, that is inversely proportional to the transition probability. The life time of transition in our calculation is approximately $2 \times 10^{-5} s$. The integral is strongly depends on the radius of the nanocrystal.

To compare with the experiments, we notice that our result for the lifetime is two orders larger than the transition lifetime in the Mn doped ZnS bulk (1.8 ms). So the extra electron injected into the quantum dot really makes the spin-forbidden transition allowable. But we do not obtain the 5 order of magnitude shortening, which is reported by Bhargava [62].

The result can be affected by many parameters. We still did not calculate the Coulomb interaction between the extra electron and the d-electrons, which can shift the energy levels and can change the transition oscillator strength[83]. And also, in this work we assume that the Mn^{2-} ion is situated at the center, which is the simplest model for our calculation. But, of course, the Mn ion can be away from the center. Then, because the spher-

ical harmonic functions will be different, the selection rule will be different, leading to the different mixing of energy levels. In this case, we may have different result for transition selection rules and transition probability. The total effect can be evaluated only when we consider all those cases.

5.8 Summary

In this Chapter, we present a theory for the entirely new model to control the optical transitions in the nanocrystal. By injecting one extra electron into the dot, one can change the transition probability and the optical properties of the nanocrystal. The mixed wavefunctions and energy level splitting were calculated in detail. This will provide the tool for further investigation of the structure and interaction of the Mn-impurity inside the nanocrystal. The rather large shortening of lifetime obtained as a numerical result shows the importance of the mechanism.

Chapter 6

CONCLUSIONS

In this thesis, we studied several important optical properties of the quantum dot and the quantum dot system.

We proposed the strain in the surface of the coated nanocrystal due to the mismatch of different lattice constants as the origin of the permanent dipole moment and the internal electric field inside the nanocrystal. We calculate the piezoelectric effect to evaluate the polarization in the surface of the nanocrystal and obtain rather large internal electric field which is comparable with experiment.

We studied the semiconductor-organic hybrid exciton , which we claim will appear when a lattice of quantum dots is embedded in the organic medium.The hyrid exciton is the result of the coupling between the "transfer" Wannier-Mott exciton, which is propagating between different dots, and the Frenkel exciton of the organic medium. The new hybrid exciton has the large exciton radius, large oscillator strength and large optical nonlinearity.

These properties can be tuned by varying dot radius, dot separation, and energies of the "bare" Wannier and Frenkel excitons.

We also present the first time a new mechanism to control the optical transitions inside the doped nanocrystal. Studying the Mn-doped ZnS quantum dot, our model investigates injecting one extra electron into the quantum dot. We calculated the exchange interaction of the extra electron with the impurity electrons at the center. The wavefunction and energy splitting were obtained in detail. As the result of this effect, the spin-forbidden transition become allowable. We obtain the shortening of lifetime of two orders of magnitude in comparison with the doped bulk. However, we do not find a shortening by 5 orders of magnitude reported by some experiments.

Chapter 7

FUTURE WORK

Due to experimental difficulties in producing a precise cubic lattice of dots, Dr. D. Norris of NEC Laboratory suggested us to consider the problem of random distribution of dots. We are planning to consider this problem in the near future. We expect that the hybrid exciton effect will remain almost the same, but the random distribution may decrease the nonlinearities.

We intend to continue the problem with the hybrid excitons. Namely, we will investigate the hybrid exciton when a single dot is embedded in the organic medium. We also intend to investigate the effect of this hybrid exciton on the medium, i.e. the change of refractive index, the interaction of this medium with light...

The Mn^{2+} doped ZnS nanocrystal will be a continuing issue. We will calculate the effect of Coulomb interaction and compare with the exchange interaction. We also want to consider the Stark effect in this nanocrystal. We also consider the interaction with the s-p electrons of the host in this

confinement geometry. We also plan to consider the case when the Mn ion is away from the center. And as some experiments reported the Mn ion in some case may seat in the surface of the nanocrystal, the problem with the Mn ion in the nanocrystal surface is worth being considered.

APPENDIX

The functions of t_2^m and e^m

Configuration	Real orbitals	Complex orbitals
t_2^1	$\|^2T_2\,\tfrac{1}{2}\xi\rangle = \|\xi^-\rangle$	$\|^2T_2\,\tfrac{1}{2}\,1\rangle = \|-1^-\rangle$
	$\|^2T_2\,\tfrac{1}{2}\eta\rangle = \|\eta^-\rangle$	$\|^2T_2\,\tfrac{1}{2}\,0\rangle = \|\zeta_0^-\rangle$
	$\|^2T_2\,\tfrac{1}{2}\zeta\rangle = \|\zeta^-\rangle$	$\|^2T_2\,\tfrac{1}{2}-1\rangle = -\|1^-\rangle$
t_2^2	$^3T_1 1x = \zeta^-\eta^-$	$\|^3T_1\,1\,1\rangle = \|-1^-\zeta_1^-\rangle$
	$^3T_1 1y = \xi^-\zeta^-$	$\|^3T_1\,1\,0\rangle = \|1^- -1^-\rangle$
	$^3T_1 1z = \eta^-\xi^-$	$\|^3T_1\,1-1\rangle = \|1^-\zeta_1^-\rangle$
	$^1A_1 = \frac{1}{\sqrt{3}}(\xi^-\eta^+ - \eta^-\zeta^+ - \zeta^-\xi^+)$	$= -\frac{1}{\sqrt{3}}(\|-1^-1^-\rangle - \|1^- -1^-\rangle + \|\zeta_0^-\zeta_0^+\rangle)$
	$^1E\theta = \frac{1}{\sqrt{6}}(\xi^-\eta^+ + \eta^-\zeta^+ - 2\zeta^-\xi^+)$	$= \frac{1}{\sqrt{6}}(-\|-1^-1^-\rangle - \|1^- -1^-\rangle + 2\|\zeta_0^-\zeta_0^+\rangle)$
	$^1E\varepsilon = \frac{1}{\sqrt{2}}(\eta^-\xi^+ - \xi^-\eta^+)$	$= \frac{1}{\sqrt{2}}(\|1^-\|-1^+\rangle - \|-1^-\|1^+\rangle)$
	$^1T_2\xi = -\frac{1}{\sqrt{2}}(\eta^-\zeta^+ + \zeta^-\eta^+)$	$\|^1T_2\,1\rangle = -\frac{1}{\sqrt{2}}(\|1^-\zeta_1^+\rangle + \|\zeta_1^-\,1^+\rangle)$
	$^1T_2\eta = -\frac{1}{\sqrt{2}}(\xi^-\zeta^+ + \zeta^-\xi^+)$	$\|^1T_2\,0\rangle = -\frac{1}{\sqrt{2}}(\|1^-\|-1^+\rangle - \|-1^-\|1^+\rangle)$
	$^1T_2\zeta = -\frac{1}{\sqrt{2}}(\xi^-\eta^+ + \eta^-\xi^+)$	$\|^1T_2\,-1\rangle = -\frac{1}{\sqrt{2}}(\|-1^-\zeta_1^+\rangle + \|\zeta_1^-\,-1^+\rangle)$
t_2^3	$^4A_2\tfrac{3}{2}x_2 = -\xi^-\eta^-\zeta^-$	$= -\|1^- -1^-\zeta_1^-\rangle$
	$^2E\,\tfrac{1}{2}\theta = \frac{1}{\sqrt{2}}(\xi^-\eta^-\zeta^+ - \xi^-\eta^+\zeta^-)$	$= -\frac{1}{\sqrt{2}}(\|1^-\zeta_1^+\rangle - \|-1^-\zeta_1^-\rangle)$
	$^2E\,\tfrac{1}{2}\varepsilon = \frac{1}{\sqrt{6}}(2\xi^-\eta^-\zeta^+ - \xi^-\eta^+\zeta^- - \xi^+\eta^-\zeta^-)$	$= \frac{1}{\sqrt{6}}(2\|1^- -1^-\zeta_1^+\rangle - \|1^- -1^+\zeta_1^-\rangle - \|1^+ -1^-\zeta_1^-\rangle)$
	$^2T_1\,\tfrac{1}{2}x = \frac{1}{\sqrt{2}}(\xi^-\eta^+ - \xi^+\eta^-)$	$\|^2T_1\,\tfrac{1}{2}\,1\rangle = \frac{1}{\sqrt{2}}(\|1^-\zeta_1^+\rangle + \|1^+ -1^-\rangle)$
	$^2T_1\,\tfrac{1}{2}y = \frac{1}{\sqrt{2}}(\eta^-\zeta^+ - \zeta^+\eta^-)$	$\|^2T_1\,\tfrac{1}{2}\,0\rangle = -\frac{1}{\sqrt{2}}(\|1^+\zeta_1^-\rangle + \|-1^+\zeta_1^-\rangle)$
	$^2T_1\,\tfrac{1}{2}z = \frac{1}{\sqrt{2}}(\zeta^-\xi^+ - \eta^+\zeta^-)$	$\|^2T_1\,\tfrac{1}{2}\,-1\rangle = -\frac{1}{\sqrt{2}}(\|-1^-\zeta_1^+\rangle + \|1^- -1^+\rangle)$
	$^2T_2\,\tfrac{1}{2}\xi = \frac{1}{\sqrt{2}}(\xi^-\zeta^+ - \zeta^-\eta^+)$	$\|^2T_2\,\tfrac{1}{2}\,1\rangle = \frac{1}{\sqrt{2}}(\|1^- -1^+\rangle - \|-1^-\zeta_1^+\rangle)$
	$^2T_2\,\tfrac{1}{2}\eta = \frac{1}{\sqrt{2}}(\eta^-\zeta^+ + \zeta^-\eta^+)$	$\|^2T_2\,\tfrac{1}{2}\,0\rangle = \frac{1}{\sqrt{2}}(\|1^- -1^-\zeta_1^+\rangle - \|1^- -1^+\zeta_1^-\rangle)$
	$^2T_2\,\tfrac{1}{2}\zeta = \frac{1}{\sqrt{2}}(\xi^-\eta^+ + \eta^-\xi^+)$	$\|^2T_2\,\tfrac{1}{2}\,-1\rangle = \frac{1}{\sqrt{2}}(\|1^-\zeta_1^+\rangle - \|1^+ -1^-\rangle)$

Configuration	Real orbitals	Complex orbitals
t_2^6	$^3T_1 1x = \xi^2\eta^-\zeta^-$	$\|^3T_1 1\,1\rangle = -\|1^- -1^2\zeta_2^-\rangle$
	$^3T_1 1y = -\xi^-\eta^2\zeta^-$	$\|^3T_1 1\,0\rangle = \|1^- -1^-\xi_1^-\rangle$
	$^3T_1 1z = \xi^-\eta^-\zeta^2$	$\|^3T_1 1\,-1\rangle = -\|1^2 -1^-\zeta_2^-\rangle$
	$^1A_1 = \frac{1}{\sqrt{3}}(\xi^2\eta^2+\eta^2\zeta^2+\zeta^2\xi^2)$	$= \frac{1}{\sqrt{3}}(-\|1^2 -1^2\rangle - \|1^- -1^-\xi_1^-\rangle + \|1^- -1^-\xi_1^-\rangle)$
	$^1E\theta = \frac{1}{\sqrt{6}}(\eta^2\zeta^2+\zeta^2\xi^2-2\xi^2\eta^2)$	$= \frac{1}{\sqrt{6}}(2\|1^2 -1^2\rangle - \|1^- -1^-\xi_1^-\rangle + \|1^- -1^-\xi_1^-\rangle)$
	$^1E\epsilon = \frac{1}{\sqrt{2}}(\xi^2\zeta^2-\eta^2\zeta^2)$	$= \frac{1}{\sqrt{2}}(\|1^2\xi_1^-\rangle + \|-1^2\xi_1^-\rangle)$
	$^1T_2\xi = \frac{1}{\sqrt{2}}(\xi^2\eta^-\zeta^- - \xi^2\eta^-\zeta^-)$	$\|^1T_2 1\rangle = \frac{1}{\sqrt{2}}(\|1^2 -1^-\zeta_1^-\rangle - \|1^2 -1^-\zeta_1^-\rangle)$
	$^1T_2\eta = \frac{1}{\sqrt{2}}(\xi^-\eta^2\zeta^- - \xi^-\eta^2\zeta^-)$	$\|^1T_2 0\rangle = \frac{1}{\sqrt{2}}(\|-1^2\xi_1^-\rangle - \|1^2\xi_1^-\rangle)$
	$^1T_2\zeta = \frac{1}{\sqrt{2}}(\xi^-\eta^-\zeta^2 - \xi^-\eta^-\zeta^2)$	$\|^1T_2 -1\rangle = \frac{1}{\sqrt{2}}(-\|1^- -1^2\zeta_1^-\rangle + \|1^- -1^2\zeta_1^-\rangle)$
t_2^5e	$^3T_2\frac{1}{2}\xi = \xi^-\eta^2\zeta^2$	$\|^3T_2\frac{1}{2}1\rangle = -\|1^- -1^2\xi_1^-\rangle$
	$^3T_2\frac{1}{2}\eta = \xi^2\eta^-\zeta^2$	$\|^3T_2\frac{1}{2}0\rangle = -\|1^2 -1^2\zeta_1^-\rangle$
	$^3T_2\frac{1}{2}\zeta = \xi^2\eta^2\zeta^-$	$\|^3T_2\frac{1}{2}-1\rangle = \|1^2 -1^-\xi_1^-\rangle$
$t_2^4e^2$	$^1A_1 = \xi^2\eta^2\zeta^2$	$= \|1^2 -1^2\xi_1^-\rangle$
e^3	$^3A_2 1\alpha_2 = \theta^-\epsilon^-$	
	$^1A_1 = \frac{1}{\sqrt{2}}(\theta^2+\epsilon^2)$	
	$^1E\theta = \frac{1}{\sqrt{2}}(\epsilon^2-\theta^2)$	
	$^1E\epsilon = \frac{1}{\sqrt{2}}(\theta^-\epsilon^- - \theta^-\epsilon^-)$	
e^3	$^2E\frac{1}{2}\theta = \theta^-\epsilon^2$	
	$^2E\frac{1}{2}\epsilon = \theta^2\epsilon^-$	
e^4	$^1A_1 = \theta^2\epsilon^2$	

Bibliography

[1] AL. L. Efros, A. L. Efros, Sov. Phys. Semicon**16**, 772 (1982)

[2] L. E. Brus, J. Chem. Phys. **80**, 4403(1982).

[3] L. Brus , J. Chem. Phys.**90**, 2555(1986)

[4] A.I. Ekimov, I. A. Kudryavtsev, M. G. Ivanov and Al. L. Efros, Sov. Phys. SolidState, **31**, 1385 (1989)

[5] J. B. Xia, Phys. Rev. B **40**, 8500(1989)

[6] L. Banyai, S. W. Koch, *Semiconductor Quantum Dots, Series on Atomic, Molecular and Optical Physics*. Vol. 2, World Scientific, Singapore, 1993.

[7] U. Wogon, *Optical Properties of Semiconductor Quantum Dots*, Springer Verlage, 1996.

[8] C. Sercel and K. J. Vahala, Phys. Rev. B**42**, 3690 (1990)

[9] A. L. Efros, Phys. Rev. B**46**, 7448 (1992).

[10] A. L. Efros and A.V. Rodina, Phys.Rev. B **47**, 10005 (1993).

[11] T. Takagahara, Phys. Rev. B474569 (1993).

[12] A. Ekimov, F. Hache, M.Schanne-Klein, D. Ricard, C. Flytzanis, I. A. Kudryavtsev, T. V. Yazeva, A. V. Rodina, Al. L. Efros, J. Opt. A. B **10**, 100(1993)

[13] E. Hanamura, Phys. Rev. B **37**, 1273 (1988).

[14] C. Kittel *Introduction to Solid State Physics*, J. Willey Co., New York,1999.

[15] G. Bastard *Wave Mechanics Applied to Semiconductor Heterostructures* New York, Wiley, 1988.

[16] S. Nomura, Y. Segawa, T. Kobayashi, Phys. Rev. B **49**, 34 (1994)

[17] D. J. Norris, A. Sacra,C. B. Murray, M. G. Bawendi, Phys. Rev. Lett. **72**, 2612 (1994),

[18] D. J. Norris and M. G. Bawendi, J. Chem. Phys.**103**, 5260 (1995)

[19] D. J. Norris and M. G. Bawendi, Phys. Rev. B**53**, 16388(1996)

[20] M. Nirmal, D. J. Norris, M. Kuno, M. G. Bawendi, A.L. Efros, M. Rosen, Phys. Rev. Lett.**75**, 3728 (1995).

[21] D. J. Norris, Al. L. Efros, M. Rosen and M. G. Bawendi, Phy. Rev. B **53**, 16347 (1996)

[22] A.L. Efros, M. Rosen, M. Kuno, M. Nirmal, D. J. Norris, M. Bawendi, Phys. Rev. B **54**, 4843 (1996).

[23] V. L. Colvin and A. P. Alivisatos, J. Chem. Phys. **97**, 730 (1992).

[24] A. P. Alivisatos, J. Phys. Chem. **100**, 13226 (1996)

[25] N. Q. Huong and J. L. Birman, J. Chem. Phys.**108**, 1769 (1998).

[26] M. E. Schmidt, S. A. Blanton, M. A. Hines and P. Guyot-Sionnest, Phys. Rev. B**53**, 12629 (1996)

[27] L. Brus "Semiconductor Colloid: Individual Nanocrystal, Opal and Porous Silicon" (unpublished)
J. Phys. Chem.**105**, 1725 (2001)

[28] J. J.Shiang, A.V. Kadavanich, R. K. Grubbs and A. P. Alivisatos, J. Phys. Chem. **99**, 17417 (1995)

[29] C. B. Murray, D. J. Norris and M. G. Bawendi, J. Am. Chem. Soc. **115**, 8706 (1993)

[30] Hines M, Guyot-Sionnest P., J. Phys. Chem **100**, 468 (1996).

[31] S.A. Empedocles, D. J. Norris, M. G.Bawendi, Phys. Rev. Lett **77**, 3873 (1996)

[32] M. A. Hines and P. Guyot-Sionnest, J. Phys. Chem.B **102**, 3655 (1998).

[33] M. E. Schmidt, S. A. Blanton, M. A. Hines and P. Guyot-Sionnest, J.Chem. Phys. **106**, 12 (1997).

[34] S. A. Blanton, R. L. Lebeny, M. A. Hines and P.Guyot-Sionnest, Phys. Rev. Lett.**79**,865 (1997); J. Phys. Chem. **99**, 17417 (1995).

[35] , M. Shim and P. Guyot-Sionnest, J. Chem. Phys. **111**, 6955 (1999).

[36] R. N. Bhargava, D. Gallagher, T. Welker, J. of Luminescence **60-61**, 275 (1994).

[37] W. Cady, Piezoelectricity ,McGraw-Hill Book Company, Inc.,New York,1946.

[38] Karl W. Boer, *Survey of Semiconductor Physics: Electron and other Particles in Bulk Semiconductors*, Van Nostrand Reinhold, New York 1990.

[39] N. Ashcroft-D. Mermin, *Solid State Physics*, Hold Rinehart Winston, 1970.

[40] We use here the bulk parameters because there are not the parameters specific for such small dots. For estimation we think the bulk parameters are resonable.

[41] X. Xeng, M. C. Schlamp, A. V. Kadavanich and A. P. Alivisatos, J. Am. Chem. Soc **119**, 7019 (1997)

[42] N. Q. Huong and J. L. Birman, J. Lum.**87-89**, 333 (2000)

[43] N. Q. Huong and J. L. Birman, Phys. Rev. **B61**, 13131 (2000).

[44] F. F. So and S. R. Forest, Phys. Rev. Lett.**66**, 2649 (1991)

[45] Y. Imanishi, S. Hattori, A. Kakuta, S. Numata, Phys. Rev. Lett.**71**, 2098 (1993)

[46] J. J.Shiang, A.V. Kadavanich, R. K. Grubbs and A. P. Alivisatos, J. Phys. Chem. **99**, 17417 (1995).

[47] C. B. Murray, C. R. Kagan, M. G. Bawendi, Science **270**, 1335 (1995).

[48] S. Facsko, T. Dekorsy, C. Koerdt, C. Trape, H. Kurz, A. Vogt, H. L. Hartnagel, Science **285**, 1551 (1999).

[49] V. Agranovich, Solid State Comm. **92**, 295 (1994).

[50] V. I. Yudson, P. Reineker, V. M. Agranovich, Phy. Rev. B, **52**, R5543 (1995).

[51] A. Engelmann, V. I. Yudson, P. Reineker, Phy. Rev. B, **57**, 1784 (1998).

[52] V. M. Agranovich, D. M. Basko, G. C. La Rocca, F. Bassani, J. Phys. Condens. Matter **10**, 9369 (1998).

[53] T. Takagahara, Solid State Comm.,**78**,No. 4, 279 (1991);

[54] Surface Science **267**, 310 (1992).

[55] T. Takagahara and E. Hanamura, Phys. Rev. Lett. **56**, 2533 (1986).

[56] S. Schmitt-Rink, D. A. B. Miller and D. S. Chemla, Phys. Rev. B **35**, 8113 (1987).

[57] L. Banyai, Y.Z. Hu, M. Lindberg, S. W. Koch, Phy. Rev. B **38**, 8142 (1988).

[58] Jackson *Classical Electrodynamics*, John Wiley and Son, 1975

[59] T. S. Moss,*Handbook on Semiconductors*, vol.1,p. 23. North-Holland Publishing Company, Amsterdam-NewYork-Oxford 1982.

[60] S.Mukamel, *Principle of Nonlinear Optical Spectroscopy*, Oxford University Press, New York-Oxford 1995.

[61] R. N. Bhargava, D. Gallagher, T. Welker, J. Lumin. **60-61**, 275 (1994).

[62] R. N. Bhargava and D. Gallagher, X. Hong and A. Nurmiko, Phys. Rev. Lett. **72**, 416 (1994).

[63] D. Gallagher, W. E. Heady, J. M. Racz, R. N. Bhargava, J. Mater. Res.**10**, 870 (1995).

[64] R. N. Bhargava, J. Lumin.**70**, 85 (1996)

[65] L. Brus, J. Quantum Electron, **22**, 1909 (1986).

[66] T. A. Kennedy, E. R. Glaser, P. B. Klein, R. N. Bhargava, Phys. Rev. B**52** R14356 (1995).

[67] Y. L. Soo, Z. H. Ming, S. W. Huang, Y. H. Kao, R. N. Bharagava, D. Gallagher, Phys. Rev. B**50**, 7602 (1994).

[68] Il Yu, T. Isobe, M. Senna, S. Takahashi, Mater. Sci. Eng.B**38**, 177 (1996).

[69] K. Sooklal, B. S. Cullum, S. M. Angel, M. J. Murphy, Phys. Chem.**100**, 4551 (1996).

[70] H. Ito, T. Tanako, T. Kuroda, F. Minami, H. Akinaga, J. Lumin **72-74**, 342 (1997)

[71] Il Yu, T. Isobe and M. Senna, J. Phys. Chem. Solids **57**, 373 (1996).

[72] M. Tanaka, J. Qi and Y. Masumoto, unpublished.

[73] V. Albe, C. Jouanin and D. Bertho, Phys. Rev. B**57**, 8778 (1998).

[74] A. A. Bol and A. Meijerink, Phys. Rev. B**58**, R15997 (1998).

[75] K.Yan, C. Duan, Y. Ma, S. Xia, J. C. Krupa, Phys. Rev. B**58**, 13585(1998)

[76] R. Parrot, C. Naud and F. Gendron, Phys. Rev. B **13**, 3748 (1976).

[77] H. E. Gumlich, J. Lumin.**23**, 73 (1981).

[78] L. A. Hemstreet, Phys. Rev. B **22**, 4590 (1980)

[79] B.Henderson and G. S. Imbusch, *Optical Spectroscopy of Inorganic Solids*, Oxford University Press, 1989.

[80] J. S. Griffith, *The Theory of Transition Metal Ions*, Cambridge University Press, 1961.

[81] P. W. Anderson, Phys. Rev. **115**, 2 (1959)

[82] Sokrates T. Pantelides, *Deep Center in Semiconductor Physics - A State-of-the-Art Approach*, Gordon and Breach Science Publishers , New York 1992

[83] K. W. H. Stevens *Magnetic Ions in Crystals*, Princeton University Press, Princeton, New Jersey 1997.